Cross-kingdom mimicry of the receptor signaling and leukocyte recruitment activity of a human cytokine by its plant orthologs

Received for publication, June 7, 2019, and in revised form, November 17, 2019 Published, Papers in Press, December 6, 2019, DOI 10.1074/jbc.RA119.009716

Dzmitry Sinitski[‡], Katrin Gruner[§], Markus Brandhofer[‡], Christos Kontos[¶], Pascal Winkler[§], Anja Reinstädler[§], Priscila Bourilhon[‡], Zhangping Xiao[‖], Robbert Cool[‖], Aphrodite Kapurniotu[¶], Frank J. Dekker[‖], Ralph Panstruga[§1], and Jürgen Bernhagen[‡2]**

*From the [‡]Chair of Vascular Biology, Institute for Stroke and Dementia Research (ISD), Klinikum der Universität München (KUM), Ludwig-Maximilians-University (LMU), 81377 Munich, Germany, the [§]Unit of Plant Molecular Cell Biology, Institute for Biology I, RWTH Aachen University, 52056 Aachen, Germany, the [¶]Division of Peptide Biochemistry, Technische Universität München (TUM), 85354 Freising, Germany, the [‖]Division of Chemical and Pharmaceutical Biology, University of Groningen, 9713 AV Groningen, The Netherlands, and the **Munich Cluster for Systems Neurology (SyNergy), 81377 Munich, Germany*

Edited by Luke O'Neill

Human macrophage migration-inhibitory factor (MIF) is an evolutionarily-conserved protein that has both extracellular immune-modulating and intracellular cell-regulatory functions. MIF plays a role in various diseases, including inflammatory diseases, atherosclerosis, autoimmunity, and cancer. It serves as an inflammatory cytokine and chemokine, but also exhibits enzymatic activity. Secreted MIF binds to cell-surface immune receptors such as CD74 and CXCR4. Plants possess MIF orthologs but lack the associated receptors, suggesting functional diversification across kingdoms. Here, we characterized three MIF orthologs (termed MIF/D-dopachrome tautomerase–like proteins or MDLs) of the model plant *Arabidopsis thaliana*. Recombinant *Arabidopsis* MDLs (*At*MDLs) share similar secondary structure characteristics with human MIF, yet only have minimal residual tautomerase activity using either *p*-hydroxyphenylpyruvate or dopachrome methyl ester as substrate. Site-specific mutagenesis suggests that this is due to a distinct amino acid difference at the catalytic cavity-defining residue Asn-98. Surprisingly, *At*MDLs bind to the human MIF receptors CD74 and CXCR4. Moreover, they activate CXCR4-dependent signaling in a receptor-specific yeast reporter system and in CXCR4-expressing human HEK293 transfectants. Notably, plant MDLs exert dose-dependent chemotactic activity toward human monocytes and T cells. A small molecule MIF inhibitor and an allosteric CXCR4 inhibitor counteract this function, revealing its specificity. Our results indicate cross-kingdom conservation of the receptor signaling and leukocyte recruitment capacities of human MIF by its plant orthologs. This may point toward a previously unrecognized interplay between plant proteins and the human innate immune system.

Chemokines are chemotactic cytokines that orchestrate immune cell trafficking in development, homeostasis, and disease. They are small polypeptides characterized by a distinctive chemokine fold and conserved N-terminal cysteine residues. According to the spacing of these cysteines, they are grouped into CC-, C*X*C-, CX_3C-, and C-type sub-classes, and correspondingly-termed chemokine receptors (CKRs)[3] exist. Chemokines interact with G-protein-coupled receptor (GPCR)-type CKRs to constitute a complex network characterized by both specificity and redundancy (1–4). Due to their major role in immune cell migration, chemokines are pivotal players in the host innate and adaptive immune response in infections, but also upon tissue injury and during tumorigenesis. When dysregulated and owing to their role in controlling leukocyte infiltration, chemokines contribute to the pathogenesis of human inflammatory and autoimmune diseases, but also cardiovascular disease and cancer (5, 6). The significance of the chemokine system to host defense against pathogens is additionally highlighted by viral mimicry mechanisms that interfere with host chemokine pathways as an immune evasion strategy (7).

Macrophage migration-inhibitory factor (MIF) is an inflammatory cytokine with chemokine-like characteristics and a regulator of host innate immunity. Dysregulated MIF has been

This work was supported by the Deutsche Forschungsgemeinschaft (DFG)-Agence Nationale Recherche (ANR) co-funded project "X-KINGDOM-MIF–cross-kingdom analysis of macrophage migration inhibitory factor (MIF) functions," DFG Grants BE1977/10-1 (to J. B.) and PA861/15-1 (to R. P.), and DFG Grant within the framework of Munich Cluster for Systems Neurology EXC 1010 SyNergy, and in part by DFG Grant SFB1123/A03 (to A. K. and J. B.). The authors declare that they have no conflicts of interest with the contents of this article.

This article contains Figs. S1–S6, Tables S1–S4, and supporting Ref. 1.

[1] To whom correspondence may be addressed: Unit of Plant Molecular Cell Biology, Institute for Biology I, RWTH Aachen University, Worringerweg 1, 52056 Aachen, Germany. Tel.: 49-241-80-26655; Fax: 49-241-80-22637; E-mail: panstruga@bio1.rwth-aachen.de.

[2] To whom correspondence may be addressed: Chair of Vascular Biology, Institute for Stroke and Dementia Research (ISD), Klinikum der Universität München (KUM), Ludwig-Maximilians-University (LMU) Munich, Feodor-Lynen-Strasse 17, 81377 Munich, Germany. Tel.: 49-89-4400–46151; Fax: 49-89-4400–46010; E-mail: juergen.bernhagen@med.uni-muenchen.de.

[3] The abbreviations used are: CKR, chemokine receptor; ACK, atypical chemokine; *At*MDL, *A. thaliana* MIF/D-DT–like protein; CD74, cluster of differentiation 74; CXCL12, C*X*C motif chemokine 12; CXCR, C*X*C motif chemokine receptor; CXCR4, C*X*C motif chemokine receptor 4; CTX, chemotactic index; D-DT, D-dopachrome tautomerase; *Hs*MIF, *Homo sapiens* MIF; HPP, *p*-hydroxyphenylpyruvate; DCME, L-dopachrome methyl ester; MHC, major histocompatibility complex; MDL, MIF/D-DT–like protein; MIF, macrophage migration-inhibitory factor; ANOVA, analysis of variance; MBP, maltose-binding protein; GPCR, G-protein–coupled receptor; HRP, horseradish peroxidase; DMEM, Dulbecco's minimal essential medium; FCS, fetal calf serum; PBMC, peripheral blood mononuclear cell; SOE-PCR, splice overlap–extension PCR; pAb, polyclonal antibody.

identified as a pivotal mediator of human diseases such as acute and chronic inflammatory diseases, autoimmunity, atherosclerosis, and cancer (8–12). MIF is a member of the emerging family of atypical chemokines (ACKs). ACKs lack the chemokine fold and the consensus cysteine residues, but behave as chemoattractants by binding to CKRs (13–15). MIF not only binds to its cognate receptor CD74 to regulate cell proliferation (16), but also engages in binding to the CKRs CXCR2 and CXCR4 (17) as well as CXCR7 (18). MIF/CXCR pathways are drivers in several human diseases. The MIF/CXCR4 signaling axis controls monocyte, T-cell, and B-cell infiltration in atherosclerosis and other inflammatory conditions (17, 19). It also contributes to cancer metastasis, cardiac fibroblast survival, and eosinophil inflammation (20, 21).

MIF is a structurally unique 12.5-kDa protein and the founding member of the MIF protein family that also comprises D-DT/MIF-2 and MIF orthologs in various species (8, 17, 22–25). MIF proteins are structurally distinct from other cytokines and classical chemokines (26), but they share high architectural homology with bacterial tautomerases (8, 13, 27–29). The coding regions of human *MIF* and its paralog *D-DT/MIF-2* are homologous and in close proximity to each other, suggesting an ancestral duplication event (24, 30). D-DT was named for its ability to tautomerize the nonnatural D-stereoisomer of dopachrome, and this catalytic property is shared by MIF (8, 27, 30). Thus, MIF proteins are bifunctional, acting as cytokines/chemokines and enzymes, although the functional significance of the tautomerase activity in mammals has remained elusive. The three-dimensional (3D) structures of MIF and D-DT/MIF-2 are highly similar (26, 31), whereas the amino acid sequence homology is limited to 34 and 27% in humans and mice, respectively. D-DT/MIF-2 shares biological and pathological activities with MIF, but also has distinct characteristics (30).

MIF proteins exhibit a remarkable degree of evolutionary conservation across kingdoms, ranging from mammals to vertebrates, including fish and unicellular parasites (8, 25, 32, 33). Mammalian MIFs are intracellularly expressed and secreted from cytosolic pools via a nonconventional secretion pathway (13). It has been speculated that MIFs are evolutionary ancient cytosolic enzymes that have "acquired" a secondary role as regulatory proteins during evolution from unicellular to multicellular organisms. Consistent with this hypothesis, intracellular MIF has been found to interact with several cytoplasmic proteins to control cell behavior by (co-)regulating cellular redox homeostasis, transcription, and signaling (13, 34). The role as a secreted cytokine/chemokine can be regarded as a further extension of its functional properties in the vertebrate lineage.

Thus, it is not surprising that interactions between MIF/receptor networks from different species/kingdoms have been reported. However, these are so far confined to interactions between a mammalian host and parasitic microbes, with MIF proteins from pathogenic species employing molecular mimicry strategies to contribute to virulence and immune evasion mechanisms (32). For example, *Plasmodium falciparum* produces a MIF ortholog that modulates the host immune response to malaria by suppressing T-cell memory (35). Similar to viral chemokine mimics, parasite MIFs appear to "hijack" host MIF receptors, albeit so far only interactions with CD74 have been reported (36, 37).

Based on sequence data bank information, the presence of MIF/D-DT–like proteins (MDLs) is also predicted in the plant kingdom, and we recently performed comprehensive *in silico* analyses of MDL genes/proteins across kingdoms and in the model plant *Arabidopsis thaliana* (*At*MDLs) (33, 38). The *A. thaliana* genome harbors three *MDL* genes, and the predicted proteins exhibit a sequence identity of 28–33% to human MIF (*Hs*MIF). A main conclusion of the *in silico* analysis has been that plant MDL proteins share residues reported to be critical for the tautomerase pocket of human MIF/D-DT and may thus have tautomerase activity (38). Interestingly, MIF orthologs from the plant-parasitic aphid *Acyrthosiphon pisum* are secreted in its saliva and mediate aphid survival and feeding on its host plant pea, representing an example of modulating plant immunity by a plant parasite. However, to date no experimental studies have been conducted with plant MDLs and their functions remain completely elusive.

Given the significant degree of sequence homology between MIFs and a predicted structural similarity across kingdoms, including a predicted conserved tautomerase site, we hypothesized that there might exist plant MIF protein-based mimicry mechanisms and that plant MDLs might interact with components of the human MIF network. To test this hypothesis, we cloned and expressed the three known *At*MDL proteins, studied their structural features by CD spectroscopy, molecular modeling, and site-specific mutagenesis, and explored functional commonalities and potential direct interactions with the human MIF protein/receptor network.

Results

Generation and characterization of His-tagged recombinant AtMDLs

To initiate functional characterization of the three predicted *At*MDL proteins *At*MDL1, *At*MDL2, and *At*MDL3 and to test the hypothesis that they might share similarities with mammalian MIFs, we recombinantly expressed these proteins and purified them for functional studies. The nucleotide and amino acid sequences of *At*MDL1, *At*MDL2, and *At*MDL3 were retrieved from UniProt and the European Nucleotide Archive (ENA) database. The *At*MDLs share a sequence identity of 28–33% with *Hs*MIF; this value is similar to the homology between human MIF and its paralog D-DT/MIF-2. For purification purposes, the *At*MDLs as well as *Hs*MIF were designed to express a C-terminal hexahistidine (6xHis) epitope tag. Table S1 summarizes key molecular parameters of the studied His-tagged proteins (*At*MDL1–6xHis, *At*MDL2–6xHis, *At*MDL3–6xHis, and *Hs*MIF–6xHis), *i.e.* the molecular mass and isoelectric points as predicted by ExPASy M_r/pI point calculator (https://web.expasy.org/compute_pi/).

The protein sequences, including the Leu–Glu linker residues and the C-terminal His-tags, were aligned using ClustalW algorithm (https://www.genome.jp/tools-bin/clustalw) (Fig. S1*A*). Prediction of the 3D structures of the *At*MDL proteins using the Phyre^2 Protein Fold Recognition Server (http://www.sbg.bio.ic.ac.uk/phyre2/html/page.cgi?id=index) suggests an

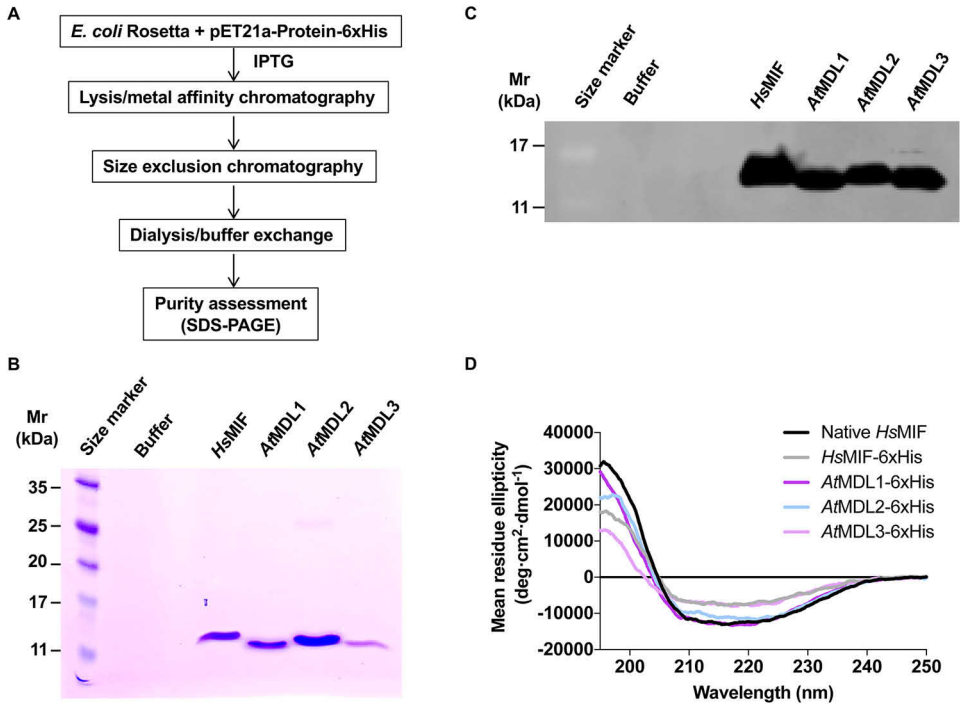

Figure 1. Expression, purification, and analysis of recombinant hexahistidine-tagged *Hs*MIF and *At*MDLs. *A,* schematic experimental procedure of protein expression and purification. *B,* Coomassie Blue staining of purified proteins after SDS-PAGE. *C,* protein detection by Western blotting using a monoclonal anti-His antibody. Relative molecular masses (M_r) are indicated on the *left* in kDa. *D,* CD spectropolarimetry of recombinant *Hs*MIF and *At*MDLs. Representative spectra of His-tagged *At*MDLs and *Hs*MIF as well as native (untagged) *Hs*MIF are presented according to the indicated color code. Conformations in the CD spectra were measured as mean residue ellipticity as a function of the wavelength (given in nanometers) in the far-UV range.

apparent high-structural similarity between the authentic (untagged) *Hs*MIF, 6xHis-tagged *Hs*MIF, and its 6xHis-tagged plant orthologs (Fig. S1*B*). To assess potential structural similarities also experimentally, *At*MDL1–6xHis, *At*MDL2–6xHis, *At*MDL3–6xHis, and *Hs*MIF–6xHis were cloned and expressed in a bacterial expression system (Fig. 1*A*). All four C-terminally His-tagged recombinant proteins were purified by immobilized metal ion affinity (HisTrap) and subsequent size-exclusion chromatography. All four proteins were obtained in good quantities, without any detectable degradation products, and in high purity of >95% as assessed by SDS-PAGE (Fig. 1*B* and Table S2), although the yield for *At*MDL3 was lower compared with the other three proteins due to an observed increased aggregation tendency. Endotoxin concentrations were found to be negligible (Table S2). The identity of the enriched proteins was validated by SDS-PAGE/Western blotting detection with an anti-His antibody (Fig. 1*C*). We additionally conducted Western blot analysis using antibodies raised against human MIF. Both the polyclonal rabbit anti-mouse MIF antibody Ka565 and the monoclonal anti-human MIF antibody MAB289 substantially cross-reacted with *At*MDL1 and also weakly bound to *At*MDL2 (Fig. S2). This result supports the notion that the *At*MDLs exhibit overlapping antigenic epitopes.

To further compare structural properties of the plant MDLs with those of *Hs*MIF, we performed circular dichroism (CD) spectroscopy. This method is a valuable tool to compare the secondary structures of proteins of interest. CD spectra of all *At*MDLs were recorded at concentrations of 1, 2.5, and 5 μM and compared with those of both His-tagged *Hs*MIF and nontagged ("fully native") *Hs*MIF (Fig. 1*D* and Fig. S3). This analysis verified that the recombinant *At*MDLs were folded and that their secondary structure was very similar to that of His-tagged *Hs*MIF and native *Hs*MIF. It also suggested that the introduced His-tag has a minimal (if any) influence on the structures of the studied proteins, as the spectral features of *Hs*MIF and *Hs*MIF–6xHis were similar at all concentrations measured (Fig. 1*D* and Fig. S3). The deconvoluted spectra recorded at a concentration of 5 μM further indicated that the proportions of secondary structure elements of the recombinant *At*MDLs differ only slightly from those of *Hs*MIF. In line with previous CD data for human and mouse MIF (39), the calculated α-helical content of the *At*MDLs was in the range of 20–37%, the β-strand contribution was between 28 and 33%, and β-turns were predicted to represent 17–22% of the secondary structural contents (Table S3). Overall, *At*MDL1–6xHis and *At*MDL2–6xHis showed the highest degree of similarity in experimentally determined secondary structural features to *Hs*MIF–6xHis; *At*MDL3–6xHis exhibited an elevated proportion of unordered secondary structural elements, an observation that is consistent with the reduced solubility of this MDL homolog compared with the other *At*MDLs and *Hs*MIF.

AtMDLs only exhibit minimal residual tautomerase activity

Whereas the functional role of the tautomerase activity of *Hs*MIF and its natural substrate in a physiological context has remained elusive, the catalytic pocket residues have also been implicated to contribute to the receptor-binding interface between MIF and its receptors CD74 and CXCR4 (12, 13, 27, 40, 41). As the *At*MDLs contain the consensus proline residue

in position 2 (Pro-2) known to be essential for tautomerase activity (Fig. S1) (38), we surmised that they may exhibit this catalytic capacity. Purified *At*MDL1–6xHis, *At*MDL2–6xHis, and *At*MDL3–6xHis were subjected to a MIF tautomerase activity assay using *p*-hydroxyphenylpyruvate (HPP) as substrate. Using a MIF concentration of 250 nM, *Hs*MIF and *Hs*MIF–6xHis exhibited a similar tautomerase activity of 80–90 μmol min^{-1} mg^{-1} (Fig. 2*A*). This value is in line with previous reports (42), indicating that the C-terminal His-tag does not interfere with the tautomerase activity of *Hs*MIF, and underscoring that the epitope-tagged variant retains structural integrity, which is consistent with previous observations made for MIF orthologs from parasites (43). Surprisingly, all three *At*MDLs were found to exhibit only minimal HPP tautomerase activity (Fig. 2*A*). Compared with buffer control conditions, the *At*MDLs at a concentration of 250 nM exhibited an apparent activity of only 1–3 μmol min^{-1} mg^{-1}, which did not differ from the control at the level of statistical significance. A more detailed comparison of the enzyme kinetics of *At*MDL1–6xHis with those of *Hs*MIF–6xHis confirmed the notion that the *At*MDLs only have minimal HPP tautomerase activity. Whereas the K_m value of the plant MDL was in the low millimolar range, *i.e.* similar to that of its human ortholog, the k_{cat} of *At*MDL1–6xHis was substantially lower than that for *Hs*MIF–6xHis, translating into a 300-fold higher k_{cat}/K_m value for *Hs*MIF–6xHis compared with the plant ortholog (Table 1). To further explore the surprising difference in tautomerase activity between *Hs*MIF and the *At*MDLs, we also compared the tautomerase activities of *At*MDL1–6xHis and *Hs*MIF–6xHis in an assay using L-dopachrome methyl ester (DCME) as substrate. At an enzyme concentration of 100 nM, *Hs*MIF–6xHis exhibited an activity of 300 μmol min^{-1} mg^{-1} toward DCME, whereas *At*MDL1–6xHis only showed an activity $<$20 μmol min^{-1} mg^{-1} (Fig. 2*B*). The notion that *At*MDL1–6xHis only has a marginal residual activity was underscored by the kinetic parameters (K_m (*Hs*MIF–6xHis) = 0.6 mM; K_m (*At*MDL1–6xHis) = 4.1 mM; k_{cat} (*Hs*MIF–6xHis) = 77.4 s^{-1}; and k_{cat} (*At*MDL1–6xHis) = 2.1 s^{-1}) with the k_{cat}/K_m value of *Hs*MIF–6xHis 250-fold higher than that of *At*MDL1–6xHis (Table 1). Thus, although the critical Pro-2 residue of the tautomerase activity site is conserved in all three *At*MDLs, the catalytic activity itself is drastically reduced in the plant orthologs of human MIF.

To begin to explore the structural basis for this striking difference, we inspected the residues that shape the catalytic tautomerase pocket (42) in 3D space more closely. We noted that in addition to Pro-2 of human MIF, Lys-32, Ile-65, and Tyr-96 are either identical or homologous in the *At*MDLs (Fig. 2*C*). By contrast, the basic His-63 residue of *Hs*MIF is substituted by a hydrophobic residue (Ile or Val) in the *At*MDLs, and even more strikingly, Asn-98 of human MIF is replaced by the strongly basic Lys-98 in all *At*MDLs, introducing a positively-charged residue in a critical position (Fig. 2*C*). The predicted 3D structures shown in Fig. 2*D* visualize the positions of residue Asn-98 *versus* Lys-98 (*top panel*; ribbon structure) and indicate that the Asn → Lys substitution may condition a conformational change of the catalytic pocket, paralleled by a different orientation of the Lys-98 side chain (*top panel*; ribbon structure, and *middle panel*; surface structure). Furthermore, the electrostatic surface potential model (Fig. 2*D*, *bottom panel*) highlights the effects of the substitutions on charge distribution around the pocket.

To experimentally test the presumed role of residue 98 for the ablated catalytic activity of the *At*MDLs, we cloned an *Hs*MIF mutant, in which Asn-98 was replaced by Lys-98. The expression and purification characteristics of N98K–*Hs*MIF–6xHis were similar to those of WT *Hs*MIF–6xHis and the hexahistidine-tagged *At*MDLs. However, when compared with WT *Hs*MIF–6xHis for its HPP- and DCME-dependent tautomerase activity, N98K–*Hs*MIF–6xHis exhibited a drastically-reduced catalytic activity (Fig. 2, *E* and *F*). Thus, the replacement of asparagine by lysine at position 98 in the *At*MDLs at least partially explains the essential absence of HPP- and DCME-dependent tautomerase activity noted in the *At*MDLs.

AtMDLs bind to and signal through human MIF receptors

The Pro-2 residue not only is a central component of the tautomerase cavity of human MIF, but also was identified to contribute to *Hs*MIF binding to the MIF receptors CD74 and CXCR4 (40, 41). Furthermore, additional motifs contributing to the binding interface between *Hs*MIF and these MIF receptors are also found in the *At*MDLs (Fig. 3*A*). Mutations in Pro-2 of *Hs*MIF have been found to invoke a conformational change in the MIF structure, resulting in altered binding and activation characteristics of CD74, suggesting that Pro-2 is a critical determinant of the MIF-binding site for CD74 (40). In addition, *Hs*MIF residues 80–87 have been identified to contribute to CD74 binding (44), and this site also is well-conserved in all three *At*MDLs (Fig. 3*A*). We therefore tested the possibility that *At*MDLs may bind to CD74, although this receptor is not present in plants. We capitalized on a recently developed MIF/CD74-binding assay that employs an MBP–sCD74 fusion protein, in which maltose-binding protein (MBP) is fused to the MIF-binding CD74 ectodomain (45). Intriguingly, all three hexahistidine-tagged *At*MDLs were found to bind to MBP–sCD74. *At*MDL3–6xHis exhibited a binding capacity that was similar to that of *Hs*MIF–6xHis (Fig. 3*B*) and bound to MBP–sCD74 with an apparent K_D of 200 nM (Fig. 3*C* and Fig. S4*A*).

For CXCR4, Pro-2 supports binding at the site 2 location of the MIF/CXCR4 interface (41, 46). Because *Hs*MIF and the *At*MDLs additionally exhibit an appreciable degree of homology in the extended N-like loop region that fosters site 1 binding of human MIF (Fig. 3*A*), we also tested the possibility that *At*MDLs may bind to human CXCR4. As GPCR ectodomains are not amenable to *in vitro* binding studies such as those performed for CD74, we employed a genetically-modified yeast transformant stably expressing human CXCR4. These cells represent a receptor-specific cell system, in which the native yeast GPCR Ste2 was replaced by human CXCR4, which is functionally linked to the yeast Ste/MAPK signaling cascade and enables us to detect receptor-specific binding and signaling responses of CXCR4 following activation with CXCL12 or MIF by β-gal reporter activity. Moreover, the system is devoid of any other mammalian receptors that might be involved in MIF signaling, thus representing a "pure" *in vivo* receptor-binding/signaling system (41, 47). Yeast CXCR4 transformants were incubated

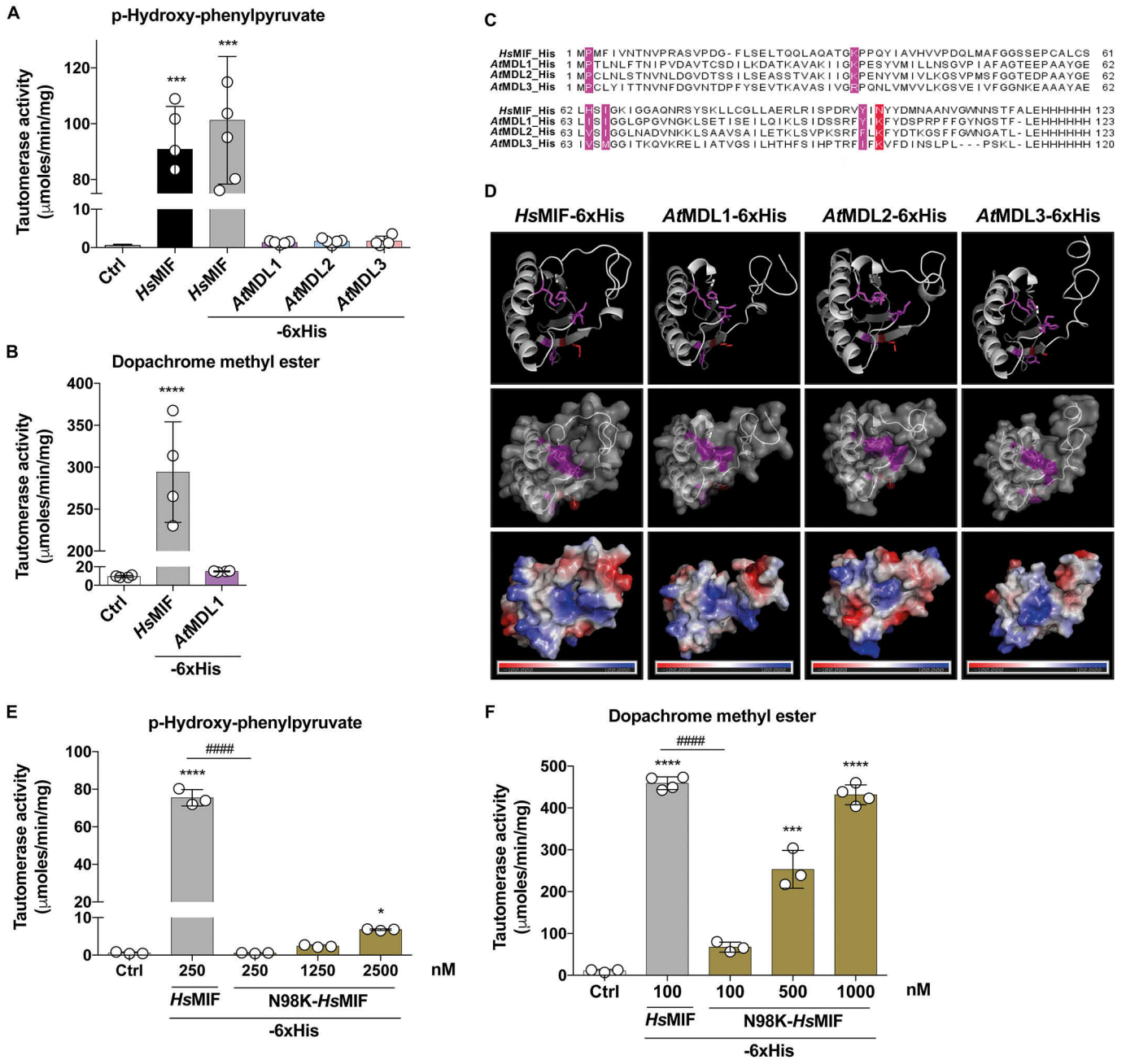

Figure 2. Recombinant *At*MDLs only have residual tautomerase activity, likely due to a sterically-impeded substrate-binding pocket. *A* and *B*, tautomerase activity of recombinant *Hs*MIF/*At*MDL protein homologs measured by spectrophotometry. *A*, tautomerase activity of the three 6xHis-tagged *At*MDLs was compared with that of 6xHis-tagged *Hs*MIF using HPP as a substrate. Untagged *Hs*MIF was measured for comparison. Data shown are from four to seven independent experiments ± S.D., each performed in triplicate (scatter plot with *white circles* indicates individual data points). For statistical comparisons, one-way ANOVA between buffer control and the different samples was applied (***, $p < 0.005$). *B*, comparison of the tautomerase activity of *At*MDL1–6xHis and *Hs*MIF–6xHis using DCME as a substrate. Data shown are from four independent experiments ± S.D., performed in triplicate each (scatter plot with *white circles* indicates individual data points). For statistical comparisons, one-way ANOVA between buffer control and the different samples was applied (***, $p < 0.005$). *C*, multiple sequence alignment of 6xHis-tagged variants of *At*MDLs and *Hs*MIF. Amino acid sequences of *At*MDL1 (identifier Q9LU69), *At*MDL2 (identifier Q9M011), *At*MDL3 (identifier Q8LG92), and *Hs*MIF (identifier P14174) were retrieved from the UniProt database and aligned by ClustalW using standard parameters in the Jalview multiple sequence alignment editor desktop application. The amino acid residues forming the tautomerase substrate-binding pocket are highlighted in *magenta* and *red*. *D*, comparative view of predicted 3D structures of 6xHis-tagged *Hs*MIF and the three *At*MDLs. Only the monomers are shown for simplicity reasons. Amino acid sequences of the *At*MDL proteins were subjected to analysis via the PHYRE^2 Fold Recognition server and visualized with PyMOL. The predicted 3D structures (ribbon, surface, and electrostatic surface potential models) of *At*MDL1–6xHis, *At*MDL2–6xHis, and *At*MDL3–6xHis were analyzed compared with the known X-ray–resolved 3D structure of *Hs*MIF–6xHis. The *upper* and *middle panels* highlight the location of crucial tautomerase pocket residues in the ribbon structure and on the protein surface (*magenta* and *red*). In the *lower panel, red* and *blue*, respectively, indicate an excess of negative or positive charges near the surface, and *grayish color* symbolizes neutral regions. *E*, comparison of the tautomerase activity of N98K–*Hs*MIF–6xHis and *Hs*MIF–6xHis using HPP as a substrate. Data shown are from three to four independent experiments ± S.D., performed in triplicate each (scatter plot with *white circles* indicates individual data points). For statistical comparisons, one-way ANOVA between buffer control and the different samples was applied (*, $p < 0.05$; ****, $p < 0.001$), as well as comparison between 250 nM *Hs*MIF and 250 nM N98K–*Hs*MIF–6xHis (####, $p < 0.001$). *F*, same as *E* except that DCME was used as a substrate, and *Hs*MIF–6xHis was applied at a concentration of 100 nM (***, $p < 0.005$; ****, $p < 0.001$; ####, $p < 0.001$).

Table 1
Comparison of the kinetic tautomerase activity parameters between recombinant His_6-tagged *Hs*MIF and *At*MDL1
Data represent triplicate measurements ± S.D.

Enzyme assay	Protein	K_m [a]	k_{cat} [b]	k_{cat}/K_m
		m_M	s^{-1}	$m_M^{-1}\,s^{-1}$
HPP	*Hs*MIF–6xHis$_6$	2.31 ± 0.86	39.78 ± 0.89	17.22
	*At*MDL1–6xHis	7.81 ± 6.63	0.44 ± 0.01	0.06
DCME	*Hs*MIF–6xHis	0.59 ± 0.18	77.39 ± 1.67	131.17
	*At*MDL1–6xHis	4.10 ± 5.19	2.11 ± 0.11	0.51

[a] K_m is the Michaelis-Menten constant.
[b] k_{cat} is turnover number.

with the recombinant *At*MDLs and their potential CXCR4 binding/signaling activity compared with that of untagged and 6xHis-tagged human MIF. CXCR4 activation by *Hs*MIF–6xHis was similar to that of *Hs*MIF, confirming that the C-terminal hexahistidine tag neither impairs nor enhances MIF binding to CXCR4 (Fig. 3*D*). In line with previous data (41), CXCR4 activation by MIF was slightly less potent than that of the cognate ligand CXCL12. Strikingly, all three *At*MDLs significantly promoted CXCR4 signaling activity. Moreover, CXCR4 activation by the plant MIF orthologs *At*MDL1–6xHis and *At*MDL3–6xHis was markedly stronger than that of *Hs*MIF–6xHis and *Hs*MIF (Fig. 3*D*).

These data suggested that *At*MDLs have the capacity to interact with the human MIF receptors CD74 and CXCR4. As the yeast CXCR4-transformant experiments also implied a role in the activation of signal transduction, we focused on CXCR4 for subsequent functional studies and next asked whether *At*MDLs would also trigger MIF-like CXCR4-facilitated signaling responses in mammalian cells. The MIF/CXCR4-induced PI3K/Akt signaling cascade is a well-studied MIF-mediated response pathway with physiological/pathophysiological relevance in human macrophages and T cells, as well as for cancer cell survival (20, 48, 49). We performed signaling studies in HEK293 cells stably overexpressing CXCR4 (HEK293–CXCR4), fostering appreciable surface expression levels of CXCR4 (Fig. S4*B*). In accordance with previous results (48), *Hs*MIF–6xHis elevated phospho-Akt levels up to 4.5-fold within 15 min of stimulation (Fig. 4, *A* and *B*). Of note, all three *At*MDLs stimulated Akt signaling in these cells. The most pronounced effect was seen for *At*MDL1–6xHis, which not only shared with human MIF the capacity to trigger Akt phosphorylation, but even exhibited a more pronounced signaling effect, with its maximum shifted to an early peak at 5 min after stimulation (Fig. 4, *C* and *D*). *At*MDL2–6xHis and *At*MDL3–6xHis had slightly weaker effects than *Hs*MIF–6xHis, and their activation maximum was delayed toward 15 min (Fig. 4, *E–H*). This result suggests that the *At*MDLs are able to mimic the CXCR4-mediated Akt phosphorylation activity of human MIF in a mammalian cell system.

Plant MIF orthologs engage CXCR4 to act as chemoattractants for human monocytes

Induction of CXCR4-dependent intracellular signaling (Figs. 3 and 4) suggests that *At*MDLs might modulate or mimic MIF's CXCR4-mediated leukocyte recruitment potential. To investigate this possibility, we tested the effect of the plant orthologs on monocyte chemotaxis, applying Transwell migration chamber experiments that represent an established setup mirroring chemokine receptor-dependent immune cell migration responses. Recombinant hexahistidine-tagged *At*MDLs were loaded into the lower compartment of a Transwell device, and their chemoattractant potency for THP-1 monocytes was compared with that of *Hs*MIF–6xHis and the classical chemokine CXCL12. In line with prior findings obtained with untagged MIF (17), *Hs*MIF–6xHis enhanced monocyte chemotaxis in a concentration-dependent manner with bell-shaped dose-response behavior and a maximal 4-fold chemotactic effect at a concentration of 16–32 nM. This compared well to the effect of the cognate CXCR4 ligand CXCL12 (chemotactic index = 4–7.5-fold compared with the untreated control at a concentration of 8 nM). Notably, all three *At*MDLs were also able to promote THP-1 cell chemotaxis, featuring dose-dependent bell-shaped behavior, albeit at slightly lower potency compared with *Hs*MIF–6xHis (Fig. 5). The maximal chemotactic effect of *At*MDL1–6xHis and *At*MDL2–6xHis was 2.5-fold compared with the buffer control and, like for *Hs*MIF–6xHis, was observed at a concentration of 32 nM. *At*MDL3–6xHis was also able to trigger monocyte migration, but its maximum effect was shifted toward a 5-fold higher concentration (chemotactic index = 3.5 at 80 nM) (Fig. 5).

We next sought to further confirm the specificity of this effect and to directly test for the involvement of CXCR4 in this process. ISO-1 is a well-established small molecule inhibitor of MIF that not only inhibits its tautomerase activity but also interferes with proinflammatory activities of MIF and MIF binding to CXCR4 (41, 50, 51). Similarly, AMD3100 is an allosteric inhibitor of CXCR4 that blocks the interaction with its cognate ligand CXCL12 and partially interferes with MIF-mediated CXCR4 activation (17, 41, 52–56). In line with these prior findings, co-application of AMD3100 fully abrogated the chemotactic effect of CXCL12 and also significantly inhibited *Hs*MIF–6xHis-mediated monocyte migration (Fig. 6 and Fig. S5). Co-application of ISO-1 blunted the effect of *Hs*MIF–6xHis, but did not interfere with CXCL12-triggered migration, confirming the specificity of MIF-driven monocyte chemotactic responses in our experimental system. Strikingly, both inhibitors completely ablated the chemotactic effect of *At*MDL1–6xHis, which was studied as a representative of the three *At*MDLs. Although not statistically significant, the drugs lowered the chemotactic effect even below baseline levels, and their effect on *At*MDL1–6xHis appeared to be even more potent than that on *Hs*MIF–6xHis. Together, these data suggested that the *At*MDLs, in particular *At*MDL1, are capable of triggering human monocyte recruitment with an efficiency similar to human MIF via interaction with the monocyte-expressed chemokine receptor CXCR4.

Plant MIF orthologs act as chemoattractants for human T cells and desensitize T-cell chemotaxis induced by human CXCL12 or MIF

THP-1 cells are monocyte-like human cells but have leukemic properties. To further test the significance of the chemotactic activity of the *At*MDLs, we wished to study primary cells to ask whether other leukocyte cell types that express CXCR4

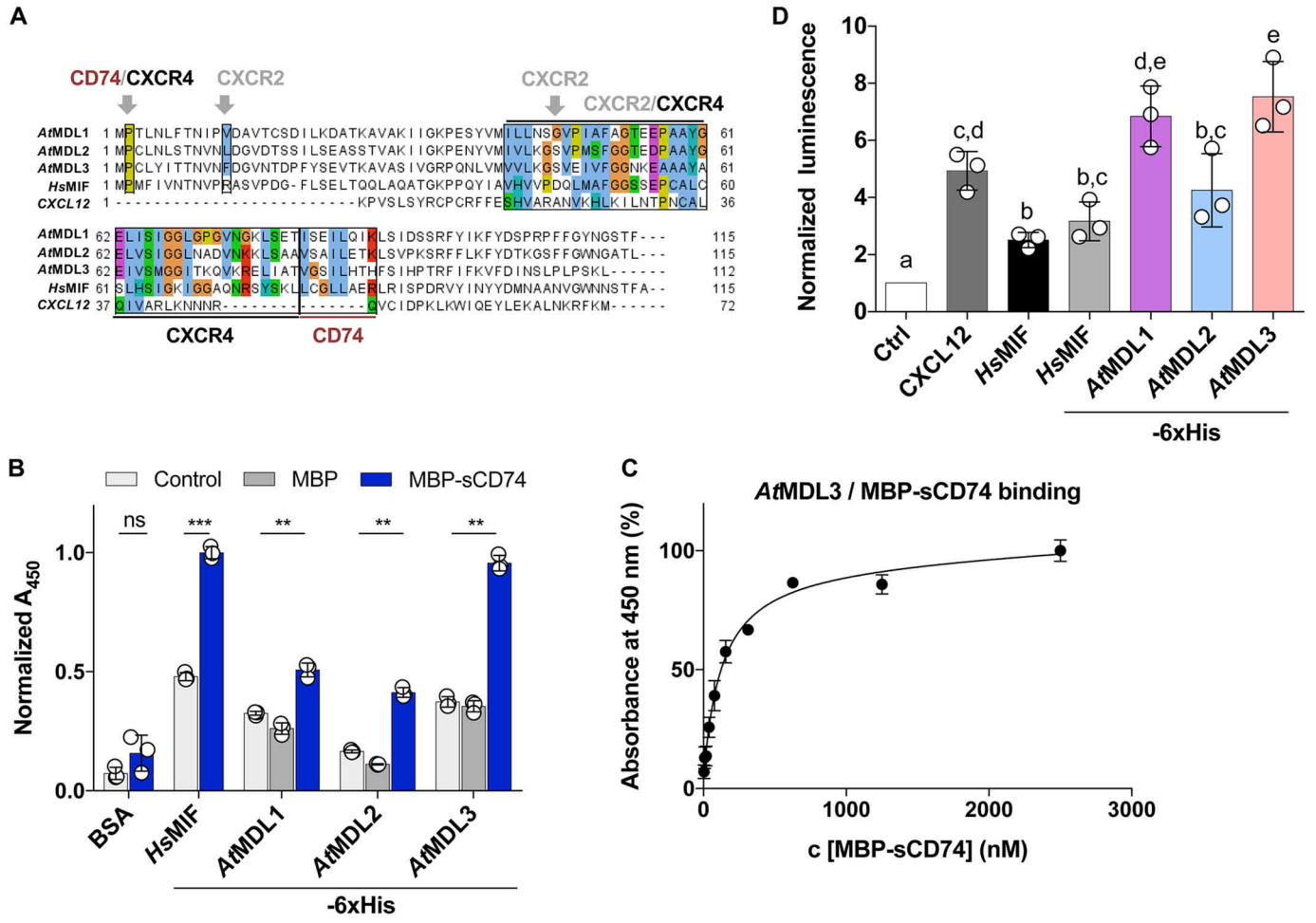

Figure 3. *At*MDLs share homology with human MIF in the MIF receptor–binding sites, bind to CD74, and activate CXCR4-mediated signaling in a yeast-based reporter system. *A,* multiple sequence alignment of the *At*MDLs, *Hs*MIF, and human CXCL12. Amino acid sequences of *At*MDL1 (identifier Q9LU69), *At*MDL2 (identifier Q9M011), *At*MDL3 (identifier Q8LG92), and *Hs*MIF (identifier P14174) were retrieved from the UniProt database and aligned by ClustalW using standard parameters in the Jalview multiple sequence alignment editor desktop application. The amino acid residues contributing to the site I and II binding interface between *Hs*MIF and CXCR4 (41) or CXCL12 and CXCR4 (90, 91), the binding sites between *Hs*MIF and CD74, and the predicted corresponding regions in the *At*MDLs are indicated. Determinants of *Hs*MIF contributing to CXCR2 binding, although not further examined in this study, are indicated for comparison. The degree of homology/identity of the MIF, CXCL12, or *At*MDL residues in these regions is highlighted by the following color score: *blue,* hydrophobic; *red*, positively charged; *magenta*, negatively charged; *green*, polar; *pink*, cysteine; *orange*, glycine; *yellow*, proline; *cyan*, aromatic; *white*, unconserved. *B*, comparison of the *in vitro* binding capacity between *Hs*MIF–6xHis and MBP–sCD74 with that of the three His-tagged *At*MDLs. Binding was measured by an ELISA-type plate-binding assay. BSA, blank PBS buffer (control), and MBP alone served as negative controls as indicated to account for nonspecific binding effects. Wells were coated with BSA (2% w/v), 500 nM *Hs*MIF, and *At*MDL1–6xHis, *At*MDL2–6xHis, and *At*MDL3–6xHis (500 nM), followed by binding of MBP or MBP–sCD74 (500 nM). After signal development, absorbance at 450 nm was measured, and the signals were normalized by setting the absorbance of *Hs*MIF as 1. *C*, curve for binding of MBP–sCD74 and *At*MDL3 using increasing concentrations of MBP–sCD74 as indicated. The data in *B* and *C* are displayed as means ± S.D. ($n = 3$); (scatter plot with *white circles* indicates individual data points); *ns*, not significant; ***, $p < 0.001$; **, $p < 0.01$. *D,* CXCR4-mediated signaling in a yeast-based reporter system. In this assay, the Ste2 GPCR of the pheromone-response pathway of *S. cerevisiae* was substituted by the human CXCR4 receptor. Ligand binding to CXCR4 triggers signaling and expression of the *lacZ* gene, as assessed by β-gal activity. The concentrations of native (untagged) *Hs*MIF, *Hs*MIF–6xHis, and His-tagged *At*MDLs were 20 μM each. The concentration of human CXCL12 was equal to 2 μM. Reporter activity is given as relative luminescence, normalized to the untreated control (*Ctrl*). Values shown represent means ± S.D. from three independent experiments, in which the activity of each was assessed in technical duplicates (scatter plot with white circles indicates individual data points). Statistical analysis was performed using one-way ANOVA and post-hoc Tukey's HSD test with multiple comparisons. *Different letters above the bars* denote a statistically significant difference between groups ($p < 0.05$), and groups showing the *same letters* are not statistically significantly different from each other.

also chemotactically respond to the *At*MDLs. Peripheral human blood-derived T cells are primary leukocytes that express substantial levels of surface CXCR4 and whose chemotactic response has been shown to be triggered by MIF (17). When examining the chemotactic migration of primary human T cells obtained from healthy donors, the dose optimum for *Hs*MIF–6xHis was found to be between 16 and 32 nM (chemotactic index = 2.3) compared with a chemotactic index of 3.5 for 8 nM CXCL12. Of note, all *At*MDLs elicited T-cell chemotaxis, and their pro-chemotactic capacity was comparable with their activity on monocyte migration, except that the optimum dose for *At*MDL1–6xHis and *At*MDL2–6xHis was at 16 nM (chemotactic index = 2–2.5) and that a significant migratory effect of *At*MDL3–6xHis was only seen at a concentration 160 nM (Fig. 7*A*). Thus, *At*MDLs also serve as chemoattractants for primary human T cells.

We employed this physiologically-relevant cell system to mechanistically explore the potential interplay between the *At*MDLs and the endogenous human CXCR4 agonists CXCL12 and MIF, hypothesizing that the plant MIF orthologs might act

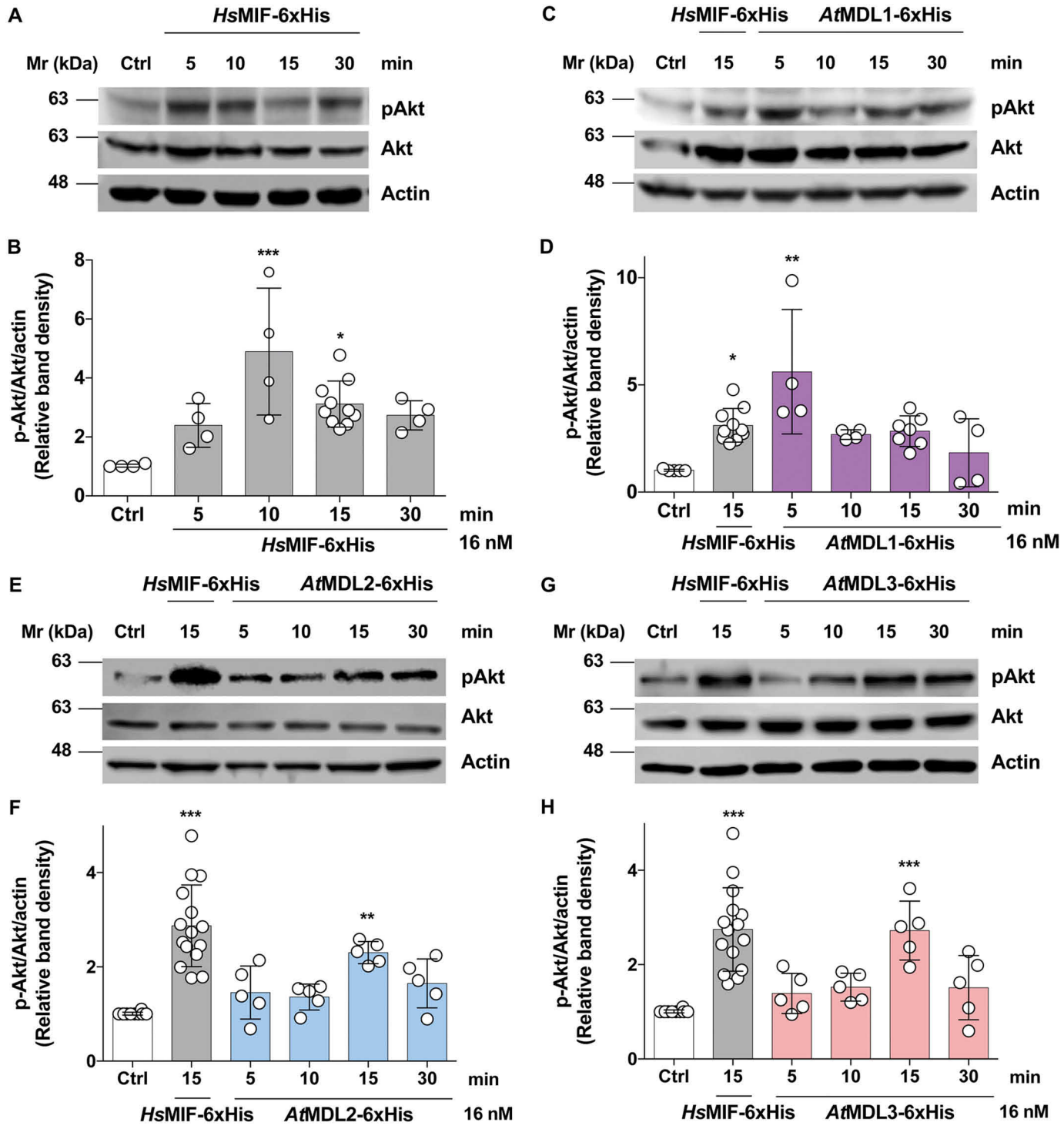

Figure 4. *At*MDLs activate the CXCR4–PI3K/Akt-signaling pathway in human CXCR4-transfected HEK293 cells. *A,* representative Western blotting indicates Akt phosphorylation (*pAkt*) at different time intervals as indicated following stimulation with *Hs*MIF–6xHis at a concentration of 16 nM. *Ctrl,* untreated control sample. Total Akt and actin were analyzed as loading control and for quantification purposes. *B,* quantification of pAkt band intensities in relation to Akt and actin band intensities according to the Western blot analysis in *A*. *Bar graph* represents means ± S.D. of 5–15 experiments (scatter plot with *white circles* indicates individual data points). Statistical analysis was performed using one-way ANOVA between the untreated control (*Ctrl*) and the various time points following treatment (*, $p < 0.05$; ***, $p < 0.005$). *C, E,* and *G,* same as *A* except that the time-dependent phosphorylation of Akt following treatment with *At*MDL1–6xHis, *At*MDL2–6xHis, and *At*MDL3–6xHis, respectively, was analyzed and compared with the effect of *Hs*MIF–6xHis at 15 min. *D, F,* and *H,* same as *B*, except that the quantification refers to the Western blot analysis in *C*, *E*, and *G* and that data are from 5 to 10 experiments (*, $p < 0.05$; **, $p < 0.01$; ***, $p < 0.005$).

to modulate T-cell chemotactic responses induced by the human agonists. We specifically asked whether the *At*MDLs would be able to enhance or desensitize T-cell chemotaxis responses triggered by the human CXCR4 chemokines. Pre-treatment with all three hexahistidine-tagged *At*MDLs added to the upper chamber of the Transwell setup fully ablated the chemoattractant activity of 16 nM *Hs*MIF–6xHis in the lower chamber (Fig. 7*B*). Similarly, all three *At*MDLs also attenuated

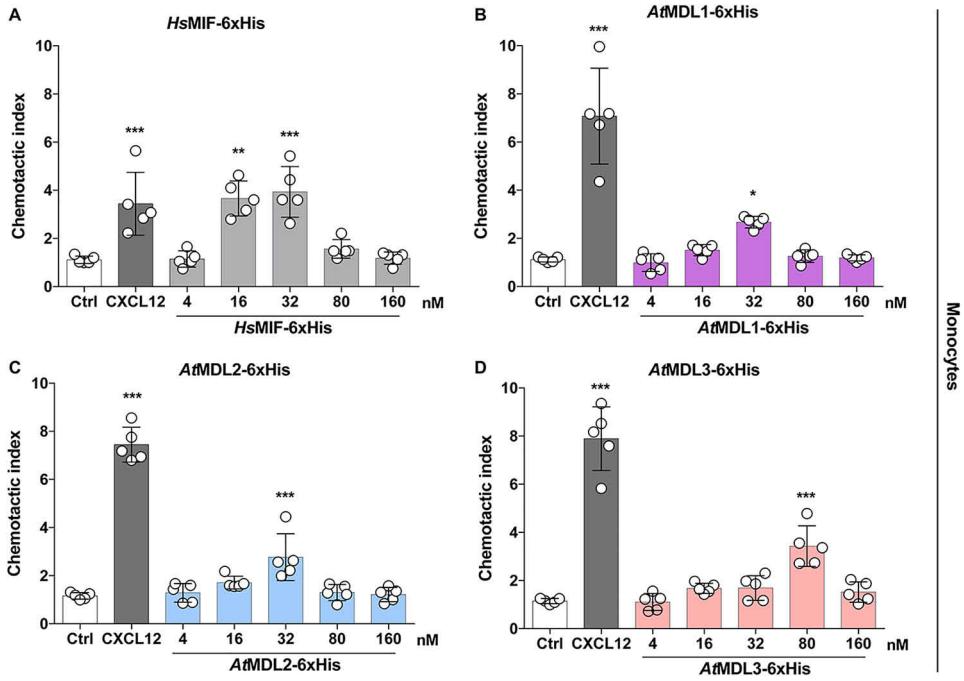

Figure 5. Recombinant 6xHis-tagged *At*MDLs trigger chemotactic migration of human THP-1 monocytes in a dose-dependent manner. Chemotaxis (referred to here as chemotactic index) of THP-1 monocytes toward *Hs*MIF–6xHis (*A*), *At*MDL1–6xHis (*B*), *At*MDL2–6xHis (*C*), or *At*MDL3–6xHis (*D*) at the different indicated concentrations. The chemotactic potency was compared with human CXCL12 (at a concentration of 8 nM) serving as a positive control and to buffer control (*Ctrl*), which also served to normalize treatments to spontaneous (random) migration events. The *bar graphs* show means ± S.D. of five independent experiments (scatter plot with *white circles* indicates individual data points). Statistical analyses were performed using one-way ANOVA between the buffer control and the treatment groups at the various doses (*, $p < 0.05$; **, $p < 0.01$; ***, $p < 0.005$).

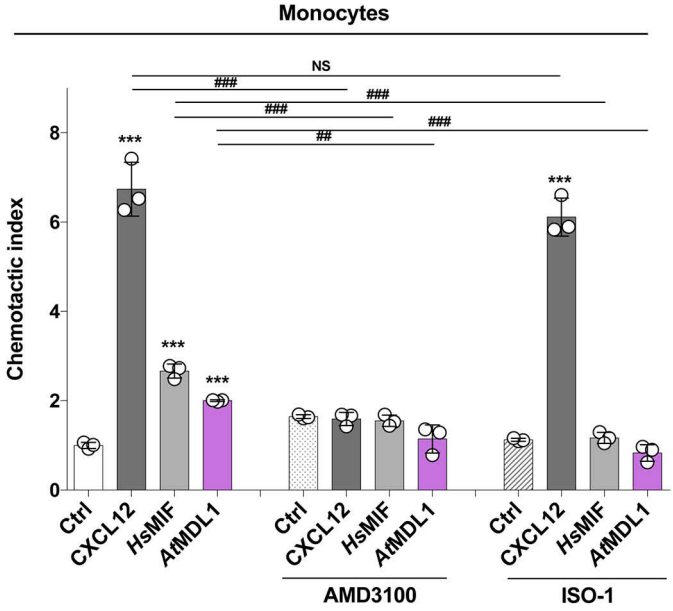

Figure 6. *At*MDL1–6xHis-triggered monocyte chemotaxis is blocked by the small molecule inhibitors AMD3100 and ISO-1, indicating MIF and CXCR4 specificity. Chemotaxis experiments were performed as shown in Fig. 5 in the absence or presence of the small molecule inhibitors AMD3100 (10 μM) or ISO-1 (100 μM) as indicated. Concentrations of the recombinant proteins were equal to 32 nM for *Hs*MIF–6xHis and *At*MDL1–6xHis and 8 nM for CXCL12. Sodium phosphate buffer was used to normalize treatments to spontaneous random migration (control, *Ctrl*). *Bar graph* shows means ± S.D. of one of two independently performed experiments carried out as technical triplicates each (for the other experiment see Fig. S5) (scatter plot with *white circles* indicates individual data points). Statistical analysis was done using one-way ANOVA for comparisons within a group (***, $p < 0.005$) and paired *t* test for comparisons between control and the AMD3100 and ISO-1 treatment groups (##, $p < 0.01$; ###, $p < 0.005$; *NS*, not significant).

the chemotactic effect of CXCL12, although full blockade was only seen for *At*MDL3–6xHis (Fig. 7*B*). As verified by an experiment adding polymyxin B, which neutralizes endotoxin, together with the *At*MDL pretreatment regimen, the desensitization effect was not due to minute endotoxin contaminants in our *At*MDL-6xHis preparations (Fig. S6). These data therefore suggested that treatment of primary human T cells with *At*MDLs desensitizes the cells for subsequent exposure to chemokines signaling through CXCR4. Plant MIF orthologs can thus directly modulate human immune cell behavior elicited by human chemokines.

Discussion

Chemokine-orchestrated immune cell trafficking is a central regulatory mechanism of the host immune response, but pathogens have developed intricate mimicry mechanisms to compromise the host chemokine system at both the ligand and receptor level. This capability is typically limited to viruses (7, 57). Prominent examples include the following: (i) lentiviridae such as HIV with the envelope protein gp120 binding to human CXCR4; (ii) γ-herpesviridae such as HHV8 that encode for the viral CC-chemokine mimic vMIP-II that functions as a chemoattractant and also binds to CXCR4; and (iii) β-herpesviridae such as human cytomegalovirus that encodes for the soluble CKR US28, serving to sequester host chemokines (7, 57, 58). Molecular mimicry of chemokines or their receptors by bacteria and fungi has not been observed, but indirect mechanisms to manipulate the host chemokine system have been reported, *e.g.* fungal mimicry of a mammalian dipeptidyl-peptidase that cleaves and inactivates CCL2 (59). Upon first view, chemokine mimicry mechanisms are counterintuitive for plants. MIF pro-

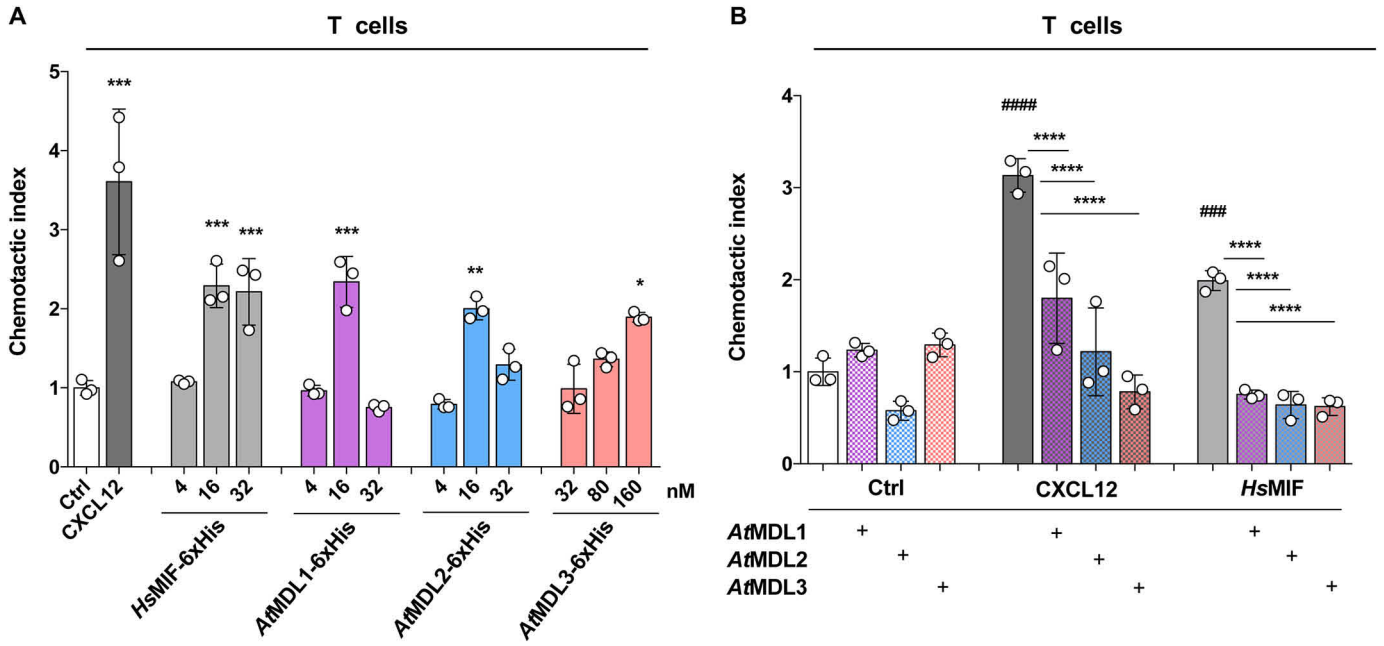

Figure 7. Recombinant 6xHis-tagged *At*MDLs dose-dependently trigger chemotactic migration of primary human T cells and desensitize T cells from CXCR4 agonist-triggered chemotaxis. *A,* recombinant 6xHis-tagged *At*MDLs trigger chemotactic migration of primary human T cells in a dose-dependent manner. The chemotactic potency was compared with *Hs*MIF–6xHis and human CXCL12 (at a concentration of 8 nM) serving as a positive control and to buffer control (*Ctrl*), which also served to normalize treatments to spontaneous (random) migration events. *Bar graphs* show means ± S.D. of three independent experiments (scatter plot with *white circles* indicates individual data points). Statistical analyses were performed using one-way ANOVA between the buffer control and the treatment groups at the various doses (*, $p < 0.05$; **, $p < 0.01$; ***, $p < 0.005$). *B,* recombinant 6xHis-tagged *At*MDLs desensitize T cells from chemotaxis elicited by CXCL12 or *Hs*MIF–6xHis. Data are the same as in *A*, except that T cells in the upper chamber were preincubated with the His-tagged *At*MDLs for 2 h (+), before being subjected to chemoattractant exposure (CXCL12 or *Hs*MIF–6xHis) in the lower chamber. Control (*Ctrl*) incubations were performed without chemoattractant in the lower chamber (random migration). *Bar graphs* show means ± S.D. of three experiments (scatter plot with white circles indicates individual data points). Statistical analyses were performed using one-way ANOVA between control and CXCL12 or *Hs*MIF (###, $p < 0.005$; ####, $p < 0.001$) and between CXCL12 or MIF with and without pre-treatment with *At*MDLs (****, $p < 0.001$).

teins are atypical chemokines that control pathogenic cell recruitment in human diseases, such as atherosclerosis and cancer through noncognate interactions with classical CKRs such as CXCR4 (8, 9, 11, 13, 17, 24, 60). CKR engagement by MIF is reminiscent of chemokine mimicry mechanisms (13). Furthermore, MIF proteins are characterized by a unique enzymatic tautomerase activity that is unprecedented in the chemokine/cytokine group of proteins and that is a notable component of the remarkable evolutionary conservation of the MIF sequence (8, 25, 61). MIF has been implicated as a player in various host–parasite interactions, and MIF orthologs have been predicted to exist even in the plant kingdom (32, 33, 38).

Here, we have cloned and experimentally characterized three MIF proteins from the model plant *A. thaliana*, *i.e. A. thaliana* MIF/D-DT–like (MDL) proteins (*At*MDLs), and we provide evidence that they are all structurally similar to human MIF (Fig. 1*D* and Figs. S1*B* and S3) and are able to mimic biological activities of human MIF (Figs. 3–7). Surprisingly, mimicry of human MIF by *At*MDLs is not related to the conserved MIF tautomerase activity, which is almost absent in *At*MDLs (Fig. 2 and Table 1), but *At*MDLs were found to interact with the human MIF receptors CD74 and CXCR4. Importantly, we discovered that they activate CXCR4-mediated Akt signaling (Fig. 4) and monocyte and T-cell chemotaxis (Figs. 5–7). These activities represent cellular functionalities of MIF typically encountered in MIF-regulated inflammatory and/or host defense responses (8, 9, 12, 25). The *At*MDLs desensitized human T cells from responding to gradients of the human CXCR4-ligating chemokines CXCL12 and MIF (Fig. 7), offering one potential mechanism of how plant MIF orthologs might influence human immunity.

Our findings indicate that *At*MDLs preserve a sufficient level of sequence conservation (Fig. 3*A*) and conformational similarity (Fig. 1*D*) to enable binding to the human MIF receptors CD74 and CXCR4, thereby allowing them to mimic functions of the endogenous human MIF or to influence human MIF or CXCL12 responses. Notably, although our experiments were only performed with MDLs from the model plant *A. thaliana*, this is to the best of our knowledge the first report demonstrating that plant proteins can phenocopy or "mimic" inflammatory activities of a *bona fide* human cytokine/chemokine.

Moreover, although plant MDLs were identified in data banks and their sequences and structures predicted by *in silico* methods (33, 38), our current study offers the first experimental characterization of plant MDLs. In fact, little is known about plant MDLs. The *in silico* analyses trace back MDLs several hundred million years in evolution and predict a role for them in plant stress-response pathways (33, 38), but an experimental validation of this presumption has been elusive. Also, there has only been a single experimental study in which plant MDL proteins have been "indirectly" implicated. Naessens *et al.* (62) previously showed that a MIF ortholog secreted in the saliva of a plant–parasitic insect modulates the immune response of the host plant. However, whether host plant MDLs are involved in this effect has remained unresolved.

To study experimentally the three predicted *At*MDLs, we opted to express these proteins recombinantly in a standard *Escherichia coli* expression system and use a C-terminal hexahistidine tag for purification purposes. Importantly, comparison of the structural and functional properties of C-terminally hexahistidine-tagged *Hs*MIF with those of native untagged *Hs*MIF in all experiments of this study essentially excludes the possibility that the hexahistidine tag artificially influences the observed mimicry effects of *At*MDLs. These findings suggest that mimicry of human MIF activities by *At*MDLs is a true property of these plant proteins.

Unique among cytokines/chemokines, MIF proteins contain a conserved tautomerase cavity that they share with the tautomerase superfamily, an evolutionarily-conserved protein family, the members of which feature an invariant N-terminal proline residue and a characteristic β–α–β-fold (28, 61). In fact, the entire 3D architecture of the MIF structure is remarkably similar to members of this family, such as the bacterial enzymes 4-oxalocrotonate tautomerase (4-OT) or 5-(carboxymethyl)-2-hydroxymuconate isomerase (CHMI), and it is similar between MIF-like proteins from different species and kingdoms, as determined by X-ray crystallographic analysis or predicted by *in silico* analyses (61). The tautomerase superfamily is characterized by catalytic promiscuity and diversity and has been suggested to be derived from a common ancestor by divergent evolution (33, 61). The known catalytic tautomerization activity of human MIF is limited to the nonnatural substrate D-dopachrome or DCME and to HPP. Whereas the keto-enol tautomerization of HPP has been generally associated with tyrosine and phenylalanine metabolism, a role for MIF in this process in mammalian cells has not been detected. Moreover, a physiological or pathophysiological relevance of the tautomerase activity of human MIF remains to be demonstrated. Nevertheless, the high degree of sequence similarity among members of the tautomerase superfamily and the conservation of the tautomerase consensus motif in plant MDLs prompted us to speculate initially that the tautomerase activity would be the basis of potential functional similarities, if any, between plant and human MIF proteins. In fact, mammalian MIF proteins have been suggested to exert dual roles with functions both in the extracellular space as cytokines/atypical chemokines and in the intracellular compartment as regulators of cell homeostasis and gene transcription (13, 34, 63). The extracellular cytokine/chemokine activities of MIF proteins are mediated by high-affinity binding to the cell-surface receptors CD74, CXCR2, and CXCR4 (and CXCR7) that are typically expressed in immune cells, and thus they represent the activities of a prototypical innate cytokine/chemokine (9, 16, 17). The molecular basis of the intracellular activities of MIF proteins is much less defined, but protein–protein-binding events and redox processes possibly also involving MIF's catalytic capacity have been implied (13, 25, 34, 63). Functional dichotomy as both the extracellular cytokine/chemokine and intracellular regulator is not unique to MIF proteins but has also been reported for proteinaceous alarmins such as the high-mobility-group box protein 1 (HMGB1) or some ribosomal tRNA transferases (13).

Given these considerations, the observed dramatic reduction in tautomerase activity of the *At*MDLs as measured in both the HPP and DCME enzymatic assays is surprising (Fig. 2, *A* and *B*). Both assays are widely applied to evaluate tautomerase activities of MIF and its variants, and *Hs*MIF–6xHis displayed full catalytic activity comparable with native untagged human MIF (Fig. 2*A*). It is likely that the almost complete lack of tautomerase activity in the *At*MDLs is a general property of these orthologs. Neither D-dopachrome nor DCME has been identified in plants, and although L-dopachrome has been implicated as a metabolite that is synthesized in some plant species and expelled via root exudates to compete out other plant species, *A. thaliana* is not a producer of this substance (64), together suggesting that dopachrome or its derivatives are unlikely to be substrates for MDLs in *Arabidopsis*. Similarly, although HPP-metabolizing enzymes have been found in plants, not much is known about the function of this metabolite, let alone its connection with MDL proteins (65). The observed marked reduction of tautomerase activity in *At*MDLs may be explained by the following mechanism. Although the K_m values of HPP and DCME are higher than that of human MIF, they are in the same order of magnitude, with a 3.5- and 8-fold lower apparent affinity for the plant MDLs, respectively (Table 1), suggesting these substrates may be capable of binding into the tautomerase pocket of *At*MDLs. However, the measured k_{cat} values indicate that catalytic conversion of both substrate types is highly inefficient in the *At*MDLs. In fact, although the overall 3D consensus motif of the tautomerase site is conserved in the three *At*MDLs, we noticed a potentially critical amino acid substitution at position 98, in which a positively-charged lysine residue in all three *At*MDLs replaces the neutral asparagine residue of *Hs*MIF (Fig. 2*C*). In fact, a model suggested by our *in silico*-modeling analysis predicting that this could trigger a conformational change and an altered charge distribution profile in the vicinity of the pocket (Fig. 2*D*) was underpinned experimentally by the generation of a site-specific mutant of human MIF, in which Asn-98 was replaced by Lys-98. N98K–*Hs*MIF showed a greatly reduced catalytic activity using both HPP and DCME as substrate (Fig. 2, *E* and *F*). Thus, the replacement of Asn-98 by Lys-98 in the *At*MDLs may be the basis for an impeded catalytic turnover in plant MDLs. Furthermore, the observed inhibitory effect of the MIF tautomerase inhibitor ISO-1, which shares structural similarities with HPP and not only fully blocked *Hs*MIF- but also *At*MDL-mediated monocyte migration (Fig. 6), furthers the notion that HPP (and DCME) binding still occurs, but that substrate tautomerization is not efficiently catalyzed by *At*MDLs. The further resolution of these mechanistic questions will have to await the 3D structural characterization of *Arabidopsis* MIF orthologs by X-ray crystallography and the elucidation of *At*MDL/inhibitor co-complexes.

In considering alternative molecular mechanisms that could give rise to functional overlaps between plant MDLs and human MIF, we explored the possibility that *At*MDLs might interact with human MIF receptors. At first glance, this appeared to be an unlikely option. Neither CD74 nor the MIF chemokine receptors CXCR2 or CXCR4 are present in plants. In fact, the existence of *bona fide* GPCRs in the plant kingdom is still controversially discussed, and it seems that only few candidates exist, none of which has been functionally linked to signaling via heterotrimeric G-proteins (66). Plants lack a cir-

culation-based immune system and deploy nonproteinaceous phytohormones such as salicylic acid, jasmonic acid, and ethylene as pivotal players for immune signaling (67). However, intriguingly, we found that *At*MDLs not only share with *Hs*MIF some degree of sequence homology regarding Pro-2 and in the site 2 binding region of the MIF/CXCR4 interface (Fig. 3*A*), but they elicited CXCR4-mediated cell signaling responses in both a yeast-based model cell system (Fig. 3*D*) and mammalian HEK293 cells (Fig. 4), comparable with the signaling effects triggered by *Hs*MIF. Moreover, the data obtained in the yeast transfectant system, which specifically expresses human CXCR4 but none of the other MIF receptors nor other mammalian proteins, argue that *At*MDLs are able to directly bind to human CXCR4. This appears surprising at first sight, but CXCR4, which was long regarded as a highly-specific chemokine receptor that only binds to one chemokine ligand, namely its cognate ligand CXCL12, has more recently been recognized to be fairly promiscuous, binding to several non-*bona fide* chemokine ligands. These include the atypical chemokine MIF, viral macrophage inflammatory protein II (vMIP-II), viral HIV gp120, human β-defensin-3 (HBD3), and extracellular ubiquitin (9, 13, 17, 56, 57,68–70). As it seems unlikely that there has been any evolutionary pressure on plant MDLs to develop agonistic properties for a human CKR, we speculate that the CXCR4-binding capacity of plant MDLs may have developed as an "evolutionary side-reaction" of plant interactions with pathogenic animals, such as recently described for plant–parasitic aphids feeding on *Nicotiana benthamiana* leaves (62). The latter scenario is somewhat reminiscent of vertebrate–parasite interactions that rely on cross-species utilization of MIF ligand/receptor pathways (71). Alternatively, the capacity of plant MDLs to activate human CKRs could be the indirect consequence of constraints imposed on MIF evolution to maintain one or several core functions of this protein family.

Although interactions between *At*MDLs and the cognate human MIF receptor CD74 were only studied by *in vitro* binding experiments on a biochemical level (Fig. 3, *B* and *C*), the data insinuate that *At*MDLs might also influence human MIF-triggered CD74 responses. On the one hand, this appears unlikely, as plants do not express a major histocompatibility (MHC) system. On the other hand, CD74 has been found to be an amenable target of parasite MIF orthologs such as leishmania, plasmodium, or hookworm (32, 35, 37, 71, 72), suggesting that it is a receptor molecule prone to be engaged during host–parasite interactions. In fact, it has been suggested that the MIF-binding functionality of CD74, which is best known as the MHC class II chaperone invariant chain Ii, already represents a "secondary" function of this membrane protein (16, 73).

Understanding the multiple functions of mammalian MIF proteins that are mediated by specific interactions with four cell-surface receptors and several intracellular-binding partners has been challenging. We have only begun to decipher the binding determinants that govern the molecular promiscuity of the interactions between MIF proteins and these binding partners (13, 17, 34, 40, 41, 46, 60, 74). Including the herein-described three *At*MDLs in corresponding comprehensive structure–activity relationship studies will add important information to the sequence and 3D motifs that specify such interactions. Accordingly, it should assist in gathering further insight for novel site-specific drug discovery approaches against human MIF that could eventually be beneficial in treating human diseases such as atherosclerosis and cancer that are at least partially mediated by MIF pathways (17, 75).

The most notable result of this study is the observation that all three *At*MDLs were found to promote monocyte and T-cell chemotactic migration (Figs. 5 and 7*A*). Moreover, the measured chemotactic effect for *At*MDL1 and -2 peaked at the same concentration as that of *Hs*MIF, albeit the chemotactic index was lower (2.5–3-fold *versus* 3.5–4-fold, respectively). Importantly, ablation of the effect by the small molecule MIF tautomerase inhibitor ISO-1 (51), which also inhibits the MIF–CXCR4 interaction (41), verified MIF specificity of the observed migration response (Fig. 6). It will be interesting to explore whether other documented small molecule MIF tautomerase inhibitors such as 4-IPP or MIF098 (25, 76) have a similar effect on *At*MDLs. Monocytes express all four MIF receptors, but pre-incubation of the monocytes with the small molecule inhibitor AMD3100, which is an established specific CXCR4 inhibitor (53) and has already been shown to partially interfere with MIF binding to CXCR4 (41), blocked the *At*MDL-mediated migration effect, providing evidence that *At*MDL-triggered monocyte chemotaxis is in fact mediated by CXCR4 (Fig. 6). T cells only express CXCR4 (as well as the relatively poorly-characterized CXCR7), but not CD74 or CXCR2, suggesting that the observed chemotaxis induced by the plant MDLs as well as the desensitization effect toward subsequent human MIF or CXCL12 chemotaxis are also mediated by CXCR4 (Fig. 7, *A* and *B*, and Fig. S6).

Thus, *At*MDLs have the surprising capacity to manipulate human immune cell motility via "hijacking" the chemokine receptor CXCR4. This raises a number of follow-up questions and hypotheses. As we already obtained biochemical-binding evidence, it could be asked whether *At*MDLs also functionally affect MIF-driven CD74 responses. Moreover, *At*MDLs might interact with CXCR2, the other chemokine receptor that human MIF engages to modulate immune cell migration and that is a prominent atherogenic arrest (77) and neutrophil recruitment receptor (78). Our results may also justify the hypothesis that MDLs from other plant species have a similar ability to engage human MIF receptors and to modulate mammalian immune cell responses.

Our study, which to the best of our knowledge shows for the first time that a plant protein with homology to a mammalian cytokine/chemokine can interact with two human cytokine receptors, may have broader implications. Following contact with plant MDLs, *e.g.* through the respiratory or the gastrointestinal tract during respiration or dietary ingestion, immune cells in the surrounding mammalian tissue might be modulated in their migratory activity by plant MDLs. Our T-cell migration desensitization data (Fig. 7) argue that this could be one mechanism how MDLs modulate human immunity. Although it is well-known that plant proteins, *e.g.* from pollen, can function as allergens to hyper-activate human adaptive immunity (79), our data may also suggest effects on components of the innate human immune system. Plant MDLs might enhance or suppress MIF-dependent innate immune responses, and this may

have a role in tissue homeostasis or in MIF-driven diseases such as acute or chronic inflammation, cardiovascular conditions, or cancer. This hypothesis will have to be tested in suitable experimental *in vivo* models in the future.

Materials and methods

Cell lines, reagents, and antibodies

The human monocytic cell line THP-1 and primary human T cells were grown in complete RPMI 1640 medium supplemented with GlutaMAX™, 10% fetal calf serum (FCS), and 1% penicillin/streptomycin. Primary human T cells were isolated from enriched peripheral blood mononuclear cell (PBMC) fractions using the human Pan T-cell isolation kit from Miltenyi Biotec (Bergisch Gladbach, Germany). PBMC fractions were obtained by apheresis via a Leucoreduction System Chamber ("Kegel") from anonymous thrombocyte donations at the Department of Transfusion Medicine, Cell Therapeutics, and Hemostaseology of the Klinikum der University Hospital (KUM) of the Ludwig-Maximilians-University (LMU). The studies abide by the Declaration of Helsinki principles and were approved by ethics approval 18-104 of the Ethics Committee of LMU Munich entitled "The MIF Protein/Receptor Network in Atherosclerosis" and encompasses the use of anonymized tissue and blood specimens for research purposes.

The human embryonic kidney cell line HEK293 was cultured in Dulbecco's minimal essential medium (DMEM) supplemented with GlutaMAX™, 10% FCS, and 1% penicillin/streptomycin. To obtain HEK293 transfectants stably expressing the human *CXC* chemokine receptor CXCR4, a high-affinity receptor for both CXCL12 and MIF, WT HEK293 cells were stably transfected with the pcDNA3.1 plasmid containing a 3xHA–*Hs*CXCR4 insert under the control of a human cytomegalovirus immediate–early promoter by an established procedure as described previously (17, 41). THP-1 monocytes, T cells, and HEK293 cells were incubated at 37 °C in a humidified atmosphere containing 5% CO_2. All cell culture reagents were cell culture grade and were obtained from Thermo Fisher Scientific (Waltham, MA).

Other reagents, *e.g.* salts, chemicals, and miscellaneous reagents, were of the highest research grade possible and were purchased from Merck KGaA (Darmstadt, Germany) and Carl Roth GmbH (Karlsruhe, Germany). Imidazole was from Sigma GmbH (Taufkirchen, Germany), and skimmed milk was from SERVA electrophoresis GmbH (Heidelberg, Germany).

Antibodies used in this study were as follows: polyclonal rabbit anti-actin (A2066; Sigma), polyclonal rabbit anti-Akt (catalog no. 9272; Cell Signaling Technologies, Danvers, MA), and polyclonal rabbit anti-phospho-Akt (Ser-473) (catalog no. 9271; Cell Signaling Technologies).

Multiple sequence alignments

Multiple sequence alignments were performed by the ClustalW algorithm (http://www.genome.jp/tools-bin/clustalw) using standard parameters in the Jalview multiple sequence alignment editor desktop application (80–82). Sources of the sequences used in the alignment are given in Table S1.

Cloning of HsMIF and the three AtMDLs with C-terminal hexahistidine tags

HsMIF and the three *A. thaliana* MIF/DDT-like (*MDL*) genes, *AtMDL1*, *AtMDL2*, and *At*MDL3, were cloned into the pET21a vector via a classical cloning strategy. The genes were N-terminally fused in-frame to a 6xHis tag present in the vector using the restriction enzymes *Nde*I and *Xho*I. For this purpose, the respective restriction sites were added to the desired cDNAs in a PCR using the corresponding primers NdeI-"gene"_Fwd and "gene"-XhoI_Rev (Table S4). The reverse primer at the same time served to remove the endogenous stop codon. For *At*MDL1 and *At*MDL3, an internal *Nde*I restriction site was removed using the splice overlap–extension PCR strategy (SOE-PCR) with the internal primer "gene"-mut_Fwd and "gene"-mut_Rev (Table S4) in combination with the above-mentioned restriction site-adding forward and reverse primers. Through the SOE-PCR, the cDNA sequences of *At*MDL1 and *At*MDL3 were modified at position 177 (GCA to GCG), introducing a silent mutation (A59A). Successfully-fused plasmid products were confirmed by sequencing, propagated in One Shot™ TOP10 chemically-competent *E. coli* (Thermo Fisher Scientific), and then transformed into Rosetta™ (DE3)-competent *E. coli* (Novagen/Merck KGaA) for expression of recombinant protein. The N98K–*Hs*MIF mutant gene was synthesized by and purchased from BaseClear (Leiden, The Netherlands). After subcloning from the pUC57 plasmid into pET21a and transformation of competent Rosetta™ (DE3) *E. coli* cells, all following procedures were identical to those described above.

Expression and purification of proteins

Recombinant nontagged human CXCL12 and *Hs*MIF proteins, used as controls in this study, were cloned, expressed, and purified as described before (46). Rosetta™ (DE3)-competent *E. coli* cells were used to express the pET21-derived gene constructs to yield *Hs*MIF–6xHis-, *At*MDL1–6xHis-, *At*MDL2–6xHis-, *At*MDL3–6xHis-, and N98K–*Hs*MIF–6xHis-tagged protein products. Culturing of bacteria and protein expression was carried out essentially as described before (46).

For protein purification, cells were harvested by centrifugation, and cell pellets were resuspended in 2 ml of binding buffer (20 mM sodium phosphate, 0.5 M NaCl, 20 mM imidazole, pH 7.2). After homogenizing the bacteria at 75 megapascals using an Aventin EmulsiFlex C5 high-pressure homogenizer (ATA Scientific Pty. Ltd., Lucas Heights, Australia), recombinant hexahistidine-tagged proteins were initially purified using immobilized metal ion affinity chromatography (HisTrap; GE Healthcare, Freiburg, Germany) with an FPLC system (FPLC; ÄKTA Pure, GE Healthcare). Prior to the run, the FLPC system was equilibrated with binding buffer. His-tagged proteins were eluted using elution buffer (20 mM sodium phosphate, 0.5 M NaCl, 0.5 M imidazole, pH 7.2). Resulting protein fractions were stored at 4 °C until subsequent purification steps or experimental usage. Additional purification of the proteins was performed by size-exclusion chromatography (Superdex 75, GE Healthcare) using 20 mM sodium phosphate buffer, pH 7.2, as elution buffer, *i.e.* conditions previously reported to support stability

and bioactivity of recombinant *Hs*MIF (17, 39). Subsequently, purified proteins were sterile-filtered using 0.2-μm pore size filters and then stored at 4 °C until use. Proteins were used for biochemical and biological assays within 4 weeks of purification. Endotoxin content was determined in the final enriched, sterile-filtered protein solution, using the Pierce™ LAL Chromogenic Endotoxin Quantitation Kit (Thermo Fisher Scientific).

Western blotting analyses of recombinant HsMIF–6xHis and AtMDL-6xHis proteins

Assessment of protein purity and integrity was performed by SDS-PAGE, using 15% acrylamide gels under reducing conditions essentially as described (39). Proteins were detected by Coomassie Blue staining and/or Western blot analysis, using nitrocellulose membranes and a Novex® Tris-glycine transfer buffer and Tris-buffered saline (TBS: 150 mM NaCl, 20 mM Tris, pH 7.3), supplemented with 0.01% Tween 20 and 1% BSA for blocking/staining. His-tagged proteins were detected by mouse anti-6xHis tag mAb (Ma1–135; Invitrogen) followed by incubation with horseradish peroxidase (HRP)-conjugated secondary goat anti-mouse IgG (ab6789; Abcam, Cambridge, UK). In addition, for testing the relative structural similarity between the mammalian and plant orthologs, anti-*Hs*MIF antibodies (anti-human MIF mAb MAB289; R&D Systems, Minneapolis, MN; anti-mouse MIF polyclonal rabbit antibody Ka565 (34)) were used, followed by HRP-conjugated secondary antibodies (catalog no. ab6789, Abcam; catalog no. P0448, DAKO) and imaging with SuperSignal™ West Dura Extended Duration Substrate (Thermo Fisher Scientific) on an Odyssey® Fc Imaging System with Image Studio™ software (LICOR Biosciences, Bad Homburg, Germany).

Far-UV CD spectroscopy

Far-UV CD spectroscopy was performed with a JASCO J-715 spectropolarimeter (JASCO, Tokyo, Japan). Measurements were carried out at room temperature between 195 and 250 nm at 0.1-nm intervals with a response time of 1 s in a buffer containing 10 mM sodium phosphate, pH 7.4. CD spectra were recorded at protein concentrations of 1, 2.5, and 5 μM in a 1-, 0.5-, or 0.2-cm quartz cuvette, respectively. The background spectrum of buffer alone was subtracted from the CD spectra of the protein solutions. The final data result from an average of three CD spectra. The CD spectra of native *Hs*MIF and their deconvolution were published previously (46) and were represented in this study for comparison after verifying similarity/identity with a representative current native *Hs*MIF preparation. Dynode voltage values were below 850 and did not interfere with CD measurements. Deconvolutions were performed using Dichroweb online software (http://dichroweb.cryst.bbk.ac.uk), and estimation of the secondary protein structure was carried out with the analysis program Contin LL, using the reference spectra Set 7 (83–86).

Tautomerase activity assays

The HPP tautomerase activity assay was performed as described before (87) with the following adjustments: 500 mM boric acid, pH 6.2, was used instead of 435 mM. Enzymatic measurements were conducted in a solution of 8 mM HPP and 250 nM of the respective recombinant protein. An increase in absorbance due to complex formation was recorded at 306 nm every 5 s for a duration of 300 s.

The DCME tautomerase activity assay was performed essentially as described before (50, 88). Briefly, DCME was prepared at a final concentration of 1 mM by oxidizing L-3,4-dihydroxyphenylalanine methyl ester with 1 mM sodium *m*-periodate. DCME was then dissolved in 25 mM potassium phosphate buffer, pH 6.0, containing 0.5 mM EDTA, and enzyme (recombinant *Hs*MIF–6xHis or *At*MDL1–6xHis) was added at a final concentration of 100 nM. The decrease in absorbance at 475 nm was measured for 240 s in 10-s intervals.

All tautomerase activity experiments were performed using a JASCO version 650 spectrophotometer (JASCO).

MBP–sCD74/MIF-binding assay

The MBP–sCD74/MIF binding assay was performed essentially as described previously (45). Briefly, freshly thawed *Hs*MIF–6xHis or *At*MDL–6xHis aliquots were diluted into phosphate-buffered saline (PBS) to prepare a solution of 500 nM from which 100 μl was used for coating the wells of a medium-binding 96-well plate overnight at 4 °C. Wells were washed three times with 220 μl of washing buffer (PBS + Tween 0.05%) and subsequently blocked for nonspecific binding with 210 μl of a commercial blocker solution (Rockland Immunochemicals Inc., Limerick, PA) at room temperature for 30 min. During all incubation steps, the plate was shaken slowly. The blocker solution was removed, and the plate was washed three times with washing buffer. Subsequently, the wells were incubated with 100 μl of a 500 nM maltose-binding protein-soluble CD74 fusion protein (MBP–sCD74) solution in PBS for 30 min at room temperature. 100 μl of PBS were used as control at this step to exclude nonspecific binding of the anti-CD74 polyclonal antibody (pAb). After washing, wells were incubated with 100 μl of a rabbit anti-CD74 pAb solution (1:2500 dilution in PBS) (Sinobiological, Vienna, Austria) for 30 min at room temperature. After removing the anti-CD74 solution and washing, a solution of 100 μl of goat anti-rabbit horseradish peroxidase conjugate (1:2000 dilution in PBS) (Life Technologies, Inc., The Netherlands) was added and incubated for 30 min at room temperature. After washing, binding was visualized by conversion of 100 μl of aqueous tetramethylbenzidine solution (Sigma, Zwijndrecht, The Netherlands), which was quenched with an aqueous 1 N H_2SO_4 solution (100 μl). Absorbance was detected at 450 nm. A freshly-prepared solution of 2% (w/v) BSA in PBS was used as negative control for coating. An additional control was done to confirm that binding between the AtMDLs and MBP–sCD74 is not caused by the fused protein MBP. Toward this aim, the incubation with MBP–sC74 was replaced by 500 nM MBP (ProSPEC Inc., Fullerton, CA) in PBS. MBP binding was detected using mouse anti-MBP mAb (1: 2500 dilution in PBS) (Sigma) as primary antibody and goat anti-mouse horseradish peroxidase conjugate (1:1500 dilution in PBS) (Thermo Fisher Scientific, Landsmeer, The Netherlands). The binding curve between *At*MDL3 with MBP–sCD74 was determined by using titrations of different concentrations of MBP–sCD74.

Yeast-signaling assay

The functional human CXCR4-expressing transformant of *S. cerevisiae* strain CY12946 was described before (46, 47). Briefly, agonist binding to the CXCR4 cell-surface receptor leads to the activation of a MAPK kinase-type signaling cascade initiating the transcription of the β-gal (*lacZ*) reporter gene. CXCR4 engagement and activation can therefore be measured and quantified by a β-gal enzymatic assay.

S. cerevisiae CY12946 cells were diluted to an OD_{600} of 0.3–0.8 and incubated with the respective test proteins (*Hs*MIF–6xHis, *At*MDL1–6xHis, *At*MDL2–6xHis, and *At*MDL3–6xHis) or the established control agonists human CXCL12 and *Hs*MIF (41, 46). All test proteins were applied at a final concentration of 20 μM, a concentration that had previously been shown to mediate MIF-based activation of CXCR4 in this system (41). CXCL12 was used at a final concentration of 2 μM. It should be noted that in this system, elevated MIF and CXCL12 ligand concentrations are needed for appreciable receptor activation due to the barrier properties of the yeast cell wall. β-Gal activity was detected using the Beta-Glo® assay system (Promega Corp., Madison, WI). Luminescence signals were recorded in a multimode plate reader (Enspire® 2300, PerkinElmer Life Sciences).

Monocyte and T-cell chemotaxis assay

The chemotactic potential of hexahistidine-tagged *At*MDL proteins was assessed using the Transwell migration device essentially as described previously (18) using THP-1 monocytes or primary human T cells and an overnight transmigration interval. THP-1 and T cells were cultured in RPMI 1640 medium supplemented with 10% FCS and 1% penicillin/streptomycin. The evening before the assay, cells were transferred into standard RPMI medium without FCS. For the assay, the upper chambers of a 24-well format Transwell device (Sigma-Corning; pore size 5 μm) were loaded with 1×10^6 THP-1 cells. Tested proteins (*Hs*MIF–6xHis, *At*MDL1–6xHis, *At*MDL2–6xHis, or *At*MDL3–6xHis) were studied at a concentration range of 4–160 nM, representing the chemoattractant in the lower chamber. As a positive control, 8 nM human CXCL12 was used; 20 mM sodium phosphate buffer, pH 7.2, served as negative control. For the desensitization experiment, 16 nM recombinant hexahistidine-tagged *At*MDLs were added to the upper T-cell–containing chamber 2 h before exposure to the chemoattractants in the lower chamber. In the endotoxin control experiment, 20 μg/ml polymyxin B was added to the upper chamber together with the *At*MDLs.

Cells that migrated into lower chambers were quantitated and obtained values normalized to buffer control ("chemotactic index") (17). The CXCR4 and MIF inhibitors AMD3100 (Sigma) and ISO-1 (Abcam, Cambridge, UK) were used at final concentrations of 10 and 100 μM, respectively, and were added to the cell suspensions 30 min before the addition of the chemotactic stimulus. Following a 16-h migration interval, cells were removed from the lower chambers, mixed with CountBright™ Absolute Counting Beads (Invitrogen/Thermo Fisher Scientific), and enumerated using a BD FACSVerse™ flow cytometer (BD Biosciences, Heidelberg, Germany).

Akt cell-signaling assay

HEK293 transfectants stably-expressing CXCR4 or non-transfected HEK293 control cells were subjected to treatment with *Hs*MIF–6xHis or *At*MDL1–6xHis, *At*MDL2–6xHis, or *At*MDL3–6xHis at a concentration of 16 nM. After different stimulation intervals, treated cells were lysed in NuPAGE® lithium dodecyl sulfate/dithiothreitol lysis buffer containing PhosSTOP™ reagent (Roche Applied Science, Mannheim, Germany). Lysates were boiled at 95 °C for 5 min, sonicated for 5 min, and electrophoresed in 11% SDS-polyacrylamide gels. For Western blotting detection of phosphorylated Akt, proteins were transferred to nitrocellulose membrane using Novex® Tris-glycine transfer buffer. Human MIF, which has been previously shown to activate Akt signaling (48), was used for comparison. Phospho-Akt band densities were determined by usage of an anti-phospho-Akt(Ser-473) antibody and an HRP-conjugated secondary antibody. Total Akt and actin were used for normalization applying polyclonal rabbit anti-Akt and -actin antibodies. Band densitometry was performed with the Odyssey® Fc imaging system (LICOR) using Image Studio™ software (LICOR Biosciences).

Fluorescence-activated cell sorting (FACS)

The cell-surface expression of the human CXCR4 receptor in HEK293 cells was verified by flow cytometry. HEK293 transfectants stably-overexpressing CXCR4 were grown in standard DMEM, supplemented with GlutaMAX™, 10% FCS, and 1% penicillin/streptomycin, until the cells reached confluence. After washing in cold phosphate-buffered saline (PBS) buffer, cells were incubated with fluorescein-isothiocyanate (FITC)-labeled mouse anti-*Hs*CXCR4 or FITC-labeled isotype control antibody (IgG2a) (both R&D Systems) at 4 °C for 2 h in the dark. Cells were washed in cold PBS before subjection to FACS analysis using a FACSVerse™ flow cytometer (BD Biosciences).

Structure prediction

Prediction of the 3D protein structures of *At*MDL1–6xHis, *At*MDL2–6xHis, and *At*MDL3–6xHis was performed using the Phyre^2 Protein Fold Recognition Server (www.sbg.bio.ic.ac.uk/phyre2) (89). Modeling was carried out in intensive mode, using the amino acid sequences obtained from public repositories (Table S1) and accounting for the His-tag–modified variants used in this study. For structure prediction and modeling, Phyre^2 performs template-based modeling together with *ab initio* folding simulations for sequence segments for which no appropriate model was found.

Structure visualization

The predicted 3D protein structures of monomeric *Hs*MIF–6xHis and *At*MDL1–6xHis, *At*MDL2–6xHis, and *At*MDL3–6xHis were visualized using the PyMOL Molecular Graphics System Version 1.8.2.2 (Schrödinger Ltd. Liability Co.). The structures shown in this work correspond to the Protein Data Bank (PDB) file for human MIF (PDB identifier 3DJH) or our structure prediction results. The 3D structures were rendered both as a cartoon model showing the secondary protein structure and as a space-filling model depicting the protein surface.

This surface model was also used to visualize the electrostatic surface potential, as calculated by PyMOL. For visualization of the three 6xHis-tagged *At*MDL proteins and their comparison with *Hs*MIF, the initial methionine residue was removed, as it has been found to be processed in all cell systems studied so far (8, 12).

Statistics

Unless otherwise indicated, statistical analyses were performed using one-way analysis of variance (ANOVA) followed by post hoc comparison with the Bonferroni test using GraphPad Prism 6 (GraphPad Prism Software Inc., San Diego, CA) with multiple comparisons. Data are presented as means ± S.D. Considered as significant: $p < 0.05$. *Asterisks* indicate statistically significant differences as follows: *, $p < 0.05$; **, $p < 0.01$; ***, $p < 0.005$; ****, $p < 0.001$. *Letter symbols above bars* in Fig. 3 indicate statistically significant different groups (at least $p < 0.05$) according to one-way ANOVA using multiple comparisons and Student's t-test.

Author contributions—D. S., K. G., M. B., C. K., P. B., and Z. X. data curation; D. S., K. G., M. B., and Z. X. formal analysis; D. S., K. G., M. B., Z. X., and R. P. visualization; D. S., K. G., C. K., P. W., A. R., P. B., Z. X., and R. H. C. methodology; D. S., K. G., M. B., C. K., P. W., A. R., P. B., Z. X., R. H. C., A. K., F. J. D., R. P., and J. B. writing-review and editing; M. B. software; R. H. C., A. K., F. J. D., R. P., and J. B. supervision; A. K., F. J. D., R. P., and J. B. conceptualization; A. K., R. P., and J. B. funding acquisition; F. J. D., R. P., and J. B. project administration; R. P. and J. B. writing original draft.

Acknowledgments—We acknowledge Christine Coustau, Harald Keller, Karl-Heinz Kogel, Richard Bucala, and Lin Leng for constructive discussions, and we thank Ying-Tung Liu for valuable assistance with the Akt phosphorylation experiments. We are grateful to the Department of Transfusion Medicine, Cell Therapeutics, and Hemostaseology of the University Hospital (KUM) of the Ludwig-Maximilians-University (LMU) for providing us with enriched PBMC fractions from thrombocyte donations to isolate primary human T cells.

References

1. Murphy, P. M., Baggiolini, M., Charo, I. F., Hébert, C. A., Horuk, R., Matsushima, K., Miller, L. H., Oppenheim, J. J., and Power, C. A. (2000) International union of pharmacology. XXII. Nomenclature for chemokine receptors. *Pharmacol. Rev.* **52,** 145–176 Medline
2. Bachelerie, F., Ben-Baruch, A., Burkhardt, A. M., Combadiere, C., Farber, J. M., Graham, G. J., Horuk, R., Sparre-Ulrich, A. H., Locati, M., Luster, A. D., Mantovani, A., Matsushima, K., Murphy, P. M., Nibbs, R., Nomiyama, H., *et al.* (2014) International Union of Basic and Clinical Pharmacology. LXXXIX. Update on the extended family of chemokine receptors and introducing a new nomenclature for atypical chemokine receptors. *Pharmacol. Rev.* **66,** 1–79 CrossRef Medline
3. Mantovani, A. (1999) The chemokine system: redundancy for robust outputs. *Immunol. Today* **20,** 254–257 CrossRef Medline
4. Steen, A., Larsen, O., Thiele, S., and Rosenkilde, M. M. (2014) Biased and G protein-independent signaling of chemokine receptors. *Front. Immunol.* **5,** 277 CrossRef Medline
5. Koenen, R. R., and Weber, C. (2011) Chemokines: established and novel targets in atherosclerosis. *EMBO Mol. Med.* **3,** 713–725 CrossRef Medline
6. Charo, I. F., and Ransohoff, R. M. (2006) The many roles of chemokines and chemokine receptors in inflammation. *N. Engl. J. Med.* **354,** 610–621 CrossRef Medline
7. Murphy, P. M. (2001) Viral exploitation and subversion of the immune system through chemokine mimicry. *Nat. Immunol.* **2,** 116–122 CrossRef Medline
8. Calandra, T., and Roger, T. (2003) Macrophage migration inhibitory factor: a regulator of innate immunity. *Nat. Rev. Immunol.* **3,** 791–800 CrossRef Medline
9. Tillmann, S., Bernhagen, J., and Noels, H. (2013) Arrest functions of the MIF ligand/receptor axes in atherogenesis. *Front. Immunol.* **4,** 115 CrossRef Medline
10. Morand, E. F., Leech, M., and Bernhagen, J. (2006) MIF: a new cytokine link between rheumatoid arthritis and atherosclerosis. *Nat. Rev. Drug Discov.* **5,** 399–410 CrossRef Medline
11. Zernecke, A., Bernhagen, J., and Weber, C. (2008) Macrophage migration inhibitory factor in cardiovascular disease. *Circulation* **117,** 1594–1602 CrossRef Medline
12. Sinitski, D., Kontos, C., Krammer, C., Asare, Y., Kapurniotu, A., and Bernhagen, J. (2019) Macrophage migration inhibitory factor (MIF)-based therapeutic concepts in atherosclerosis and inflammation. *Thromb. Haemost.* **119,** 553–566 CrossRef Medline
13. Kapurniotu, A., Gokce, O., and Bernhagen, J. (2019) The multitasking potential of alarmins and atypical chemokines. *Front. Med.* **6,** 3 CrossRef Medline
14. Noels, H., Bernhagen, J., and Weber, C. (2009) Macrophage migration inhibitory factor: a noncanonical chemokine important in atherosclerosis. *Trends Cardiovasc. Med.* **19,** 76–86 CrossRef Medline
15. Oppenheim, J. J., Tewary, P., de la Rosa, G., and Yang, D. (2007) Alarmins initiate host defense. *Adv. Exp. Med. Biol.* **601,** 185–194 CrossRef Medline
16. Leng, L., Metz, C. N., Fang, Y., Xu, J., Donnelly, S., Baugh, J., Delohery, T., Chen, Y., Mitchell, R. A., and Bucala, R. (2003) MIF signal transduction initiated by binding to CD74. *J. Exp. Med.* **197,** 1467–1476 CrossRef Medline
17. Bernhagen, J., Krohn, R., Lue, H., Gregory, J. L., Zernecke, A., Koenen, R. R., Dewor, M., Georgiev, I., Schober, A., Leng, L., Kooistra, T., Fingerle-Rowson, G., Ghezzi, P., Kleemann, R., McColl, S. R., *et al.* (2007) MIF is a noncognate ligand of CXC chemokine receptors in inflammatory and atherogenic cell recruitment. *Nat. Med.* **13,** 587–596 CrossRef Medline
18. Alampour-Rajabi, S., El Bounkari, O., Rot, A., Müller-Newen, G., Bachelerie, F., Gawaz, M., Weber, C., Schober, A., and Bernhagen, J. (2015) MIF interacts with CXCR7 to promote receptor internalization, ERK1/2 and ZAP-70 signaling, and lymphocyte chemotaxis. *FASEB J.* **29,** 4497–4511 CrossRef Medline
19. Schmitz, C., Noels, H., El Bounkari, O., Straussfeld, E., Megens, R. T. A., Sternkopf, M., Alampour-Rajabi, S., Krammer, C., Tilstam, P. V., Gerdes, N., Bürger, C., Kapurniotu, A., Bucala, R., Jankowski, J., Weber, C., and Bernhagen, J. (2018) Mif-deficiency favors an atheroprotective autoantibody phenotype in atherosclerosis. *FASEB J.* **32,** 4428–4443 CrossRef Medline
20. Soppert, J., Kraemer, S., Beckers, C., Averdunk, L., Möllmann, J., Denecke, B., Goetzenich, A., Marx, G., Bernhagen, J., and Stoppe, C. (2018) Soluble CD74 reroutes MIF/CXCR4/AKT-mediated survival of cardiac myofibroblasts to necroptosis. *J. Am. Heart Assoc.* **7,** e009384 CrossRef Medline
21. de Souza, H. S., Tortori, C. A., Lintomen, L., Figueiredo, R. T., Bernardazzi, C., Leng, L., Bucala, R., Madi, K., Buongusto, F., Elia, C. C., Castelo-Branco, M. T., and Bozza, M. T. (2015) Macrophage migration inhibitory factor promotes eosinophil accumulation and tissue remodeling in eosinophilic esophagitis. *Mucosal Immunol.* **8,** 1154–1165 CrossRef Medline
22. David, J. R. (1966) Delayed hypersensitivity in vitro: its mediation by cell-free substances formed by lymphoid cell-antigen interaction. *Proc. Natl. Acad. Sci. U.S.A.* **56,** 72–77 CrossRef Medline
23. Bernhagen, J., Calandra, T., Mitchell, R. A., Martin, S. B., Tracey, K. J., Voelter, W., Manogue, K. R., Cerami, A., and Bucala, R. (1993) MIF is a pituitary-derived cytokine that potentiates lethal endotoxaemia. *Nature* **365,** 756–759 CrossRef Medline
24. Merk, M., Mitchell, R. A., Endres, S., and Bucala, R. (2012) D-Dopachrome tautomerase (D-DT or MIF-2): doubling the MIF cytokine family. *Cytokine* **59,** 10–17 CrossRef Medline

25. Bloom, J., Sun, S., and Al-Abed, Y. (2016) MIF, a controversial cytokine: a review of structural features, challenges, and opportunities for drug development. *Exp. Opin. Ther. Targets* **20,** 1463–1475 CrossRef Medline
26. Sun, H. W., Bernhagen, J., Bucala, R., and Lolis, E. (1996) Crystal structure at 2.6-A resolution of human macrophage migration inhibitory factor. *Proc. Natl. Acad. Sci. U.S.A.* **93,** 5191–5196 CrossRef Medline
27. Lolis, E., and Bucala, R. (2003) Macrophage migration inhibitory factor. *Exp. Opin. Ther. Targets* **7,** 153–164 CrossRef Medline
28. Stamps, S. L., Fitzgerald, M. C., and Whitman, C. P. (1998) Characterization of the role of the amino-terminal proline in the enzymatic activity catalyzed by macrophage migration inhibitory factor. *Biochemistry* **37,** 10195–10202 CrossRef Medline
29. Taylor, A. B., Johnson, W. H., Jr, Czerwinski, R. M., Li, H. S., Hackert, M. L., and Whitman, C. P. (1999) Crystal structure of macrophage migration inhibitory factor complexed with (E)-2-fluoro-*p*-hydroxycinnamate at 1.8 Å resolution: implications for enzymatic catalysis and inhibition. *Biochemistry* **38,** 7444–7452 CrossRef Medline
30. Merk, M., Zierow, S., Leng, L., Das, R., Du, X., Schulte, W., Fan, J., Lue, H., Chen, Y., Xiong, H., Chagnon, F., Bernhagen, J., Lolis, E., Mor, G., Lesur, O., and Bucala, R. (2011) The D-Dopachrome tautomerase (DDT) gene product is a cytokine and functional homolog of macrophage migration inhibitory factor (MIF). *Proc. Natl. Acad. Sci. U.S.A.* **108,** E577–E585 CrossRef Medline
31. Sugimoto, H., Taniguchi, M., Nakagawa, A., Tanaka, I., Suzuki, M., and Nishihira, J. (1999) Crystal structure of human D-dopachrome tautomerase, a homologue of macrophage migration inhibitory factor, at 1.54 A resolution. *Biochemistry* **38,** 3268–3279 CrossRef Medline
32. Sparkes, A., De Baetselier, P., Roelants, K., De Trez, C., Magez, S., Van Ginderachter, J. A., Raes, G., Bucala, R., and Stijlemans, B. (2017) The non-mammalian MIF superfamily. *Immunobiology* **222,** 473–482 CrossRef Medline
33. Michelet, C., Danchin, E. G. J., Jaouannet, M., Bernhagen, J., Panstruga, R., Kogel, K. H., Keller, H., and Coustau, C. (2019) Cross-kingdom analysis of diversity, evolutionary history, and site selection within the eukaryotic macrophage migration inhibitory factor superfamily. *Genes* **10,** E740 CrossRef Medline
34. Kleemann, R., Hausser, A., Geiger, G., Mischke, R., Burger-Kentischer, A., Flieger, O., Johannes, F. J., Roger, T., Calandra, T., Kapurniotu, A., Grell, M., Finkelmeier, D., Brunner, H., and Bernhagen, J. (2000) Intracellular action of the cytokine MIF to modulate AP-1 activity and the cell cycle through Jab1. *Nature* **408,** 211–216 CrossRef Medline
35. Baeza Garcia, A., Siu, E., Sun, T., Exler, V., Brito, L., Hekele, A., Otten, G., Augustijn, K., Janse, C. J., Ulmer, J. B., Bernhagen, J., Fikrig, E., Geall, A., and Bucala, R. (2018) Neutralization of the *Plasmodium*-encoded MIF ortholog confers protective immunity against malaria infection. *Nat. Commun.* **9,** 2714 CrossRef Medline
36. Twu, O., Dessí, D., Vu, A., Mercer, F., Stevens, G. C., de Miguel, N., Rappelli, P., Cocco, A. R., Clubb, R. T., Fiori, P. L., and Johnson, P. J. (2014) *Trichomonas vaginalis* homolog of macrophage migration inhibitory factor induces prostate cell growth, invasiveness, and inflammatory responses. *Proc. Natl. Acad. Sci. U.S.A.* **111,** 8179–8184 CrossRef Medline
37. Kamir, D., Zierow, S., Leng, L., Cho, Y., Diaz, Y., Griffith, J., McDonald, C., Merk, M., Mitchell, R. A., Trent, J., Chen, Y., Kwong, Y. K., Xiong, H., Vermeire, J., Cappello, M., *et al.* (2008) A *Leishmania* ortholog of macrophage migration inhibitory factor modulates host macrophage responses. *J. Immunol.* **180,** 8250–8261 CrossRef Medline
38. Panstruga, R., Baumgarten, K., and Bernhagen, J. (2015) Phylogeny and evolution of plant macrophage migration inhibitory factor/D-dopachrome tautomerase-like proteins. *BMC Evolut. Biol.* **15,** 64 CrossRef Medline
39. Bernhagen, J., Mitchell, R. A., Calandra, T., Voelter, W., Cerami, A., and Bucala, R. (1994) Purification, bioactivity, and secondary structure analysis of mouse and human macrophage migration inhibitory factor (MIF). *Biochemistry* **33,** 14144–14155 CrossRef Medline
40. Pantouris, G., Syed, M. A., Fan, C., Rajasekaran, D., Cho, T. Y., Rosenberg, E. M., Jr, Bucala, R., Bhandari, V., and Lolis, E. J. (2015) An analysis of MIF structural features that control functional activation of CD74. *Chem. Biol.* **22,** 1197–1205 CrossRef Medline
41. Rajasekaran, D., Gröning, S., Schmitz, C., Zierow, S., Drucker, N., Bakou, M., Kohl, K., Mertens, A., Lue, H., Weber, C., Xiao, A., Luker, G., Kapurniotu, A., Lolis, E., and Bernhagen, J. (2016) Macrophage migration inhibitory factor-CXCR4 receptor interactions: evidence for partial allosteric agonism in comparison with CXCL12 chemokine. *J. Biol. Chem.* **291,** 15881–15895 CrossRef Medline
42. Lubetsky, J. B., Swope, M., Dealwis, C., Blake, P., and Lolis, E. (1999) Pro-1 of macrophage migration inhibitory factor functions as a catalytic base in the phenylpyruvate tautomerase activity. *Biochemistry* **38,** 7346–7354 CrossRef Medline
43. Sommerville, C., Richardson, J. M., Williams, R. A., Mottram, J. C., Roberts, C. W., Alexander, J., and Henriquez, F. L. (2013) Biochemical and immunological characterization of *Toxoplasma gondii* macrophage migration inhibitory factor. *J. Biol. Chem.* **288,** 12733–12741 CrossRef Medline
44. Assis, D. N., Leng, L., Du, X., Zhang, C. K., Grieb, G., Merk, M., Garcia, A. B., McCrann, C., Chapiro, J., Meinhardt, A., Mizue, Y., Nikolic-Paterson, D. J., Bernhagen, J., Kaplan, M. M., Zhao, H., *et al.* (2014) The role of macrophage migration inhibitory factor in autoimmune liver disease. *Hepatology* **59,** 580–591 CrossRef Medline
45. Kok, T., Wasiel, A. A., Dekker, F. J., Poelarends, G. J., and Cool, R. H. (2018) High yield production of human invariant chain CD74 constructs fused to solubility-enhancing peptides and characterization of their MIF-binding capacities. *Protein Expr. Purif.* **148,** 46–53 CrossRef Medline
46. Lacy, M., Kontos, C., Brandhofer, M., Hille, K., Gröning, S., Sinitski, D., Bourilhon, P., Rosenberg, E., Krammer, C., Thavayogarajah, T., Pantouris, G., Bakou, M., Weber, C., Lolis, E., Bernhagen, J., and Kapurniotu, A. (2018) Identification of an Arg-Leu-Arg tripeptide that contributes to the binding interface between the cytokine MIF and the chemokine receptor CXCR4. *Sci. Rep.* **8,** 5171 CrossRef Medline
47. Sachpatzidis, A., Benton, B. K., Manfredi, J. P., Wang, H., Hamilton, A., Dohlman, H. G., and Lolis, E. (2003) Identification of allosteric peptide agonists of CXCR4. *J. Biol. Chem.* **278,** 896–907 CrossRef Medline
48. Lue, H., Thiele, M., Franz, J., Dahl, E., Speckgens, S., Leng, L., Fingerle-Rowson, G., Bucala, R., Lüscher, B., and Bernhagen, J. (2007) Macrophage migration inhibitory factor (MIF) promotes cell survival by activation of the Akt pathway and role for CSN5/JAB1 in the control of autocrine MIF activity. *Oncogene* **26,** 5046–5059 CrossRef Medline
49. Schwartz, V., Lue, H., Kraemer, S., Korbiel, J., Krohn, R., Ohl, K., Bucala, R., Weber, C., and Bernhagen, J. (2009) A functional heteromeric MIF receptor formed by CD74 and CXCR4. *FEBS Lett.* **583,** 2749–2757 CrossRef Medline
50. Lubetsky, J. B., Dios, A., Han, J., Aljabari, B., Ruzsicska, B., Mitchell, R., Lolis, E., and Al-Abed, Y. (2002) The tautomerase active site of macrophage migration inhibitory factor is a potential target for discovery of novel anti-inflammatory agents. *J. Biol. Chem.* **277,** 24976–24982 CrossRef Medline
51. Al-Abed, Y., Dabideen, D., Aljabari, B., Valster, A., Messmer, D., Ochani, M., Tanovic, M., Ochani, K., Bacher, M., Nicoletti, F., Metz, C., Pavlov, V. A., Miller, E. J., and Tracey, K. J. (2005) ISO-1 binding to the tautomerase active site of MIF inhibits its pro-inflammatory activity and increases survival in severe sepsis. *J. Biol. Chem.* **280,** 36541–36544 CrossRef Medline
52. De Clercq, E. (2003) The bicyclam AMD3100 story. *Nat. Rev. Drug Discov.* **2,** 581–587 CrossRef Medline
53. Burger, J. A., and Stewart, D. J. (2009) CXCR4 chemokine receptor antagonists: perspectives in SCLC. *Exp. Opin. Investig. Drugs* **18,** 481–490 CrossRef Medline
54. Kessans, M. R., Gatesman, M. L., and Kockler, D. R. (2010) Plerixafor: a peripheral blood stem cell mobilizer. *Pharmacotherapy* **30,** 485–492 CrossRef Medline
55. De Clercq, E. (2015) AMD3100/CXCR4 inhibitor. *Front. Immunol.* **6,** 276 CrossRef Medline
56. Pawig, L., Klasen, C., Weber, C., Bernhagen, J., and Noels, H. (2015) Diversity and inter-connections in the CXCR4 chemokine receptor/ligand family: molecular perspectives. *Front. Immunol.* **6,** 429 CrossRef Medline
57. Qin, L., Kufareva, I., Holden, L. G., Wang, C., Zheng, Y., Zhao, C., Fenalti, G., Wu, H., Han, G. W., Cherezov, V., Abagyan, R., Stevens, R. C., and

Handel, T. M. (2015) Structural biology. Crystal structure of the chemokine receptor CXCR4 in complex with a viral chemokine. *Science* **347,** 1117–1122 CrossRef Medline
58. Szpakowska, M., and Chevigné, A. (2016) vCCL2/vMIP-II, the viral master KEYmokine. *J. Leukoc. Biol.* **99,** 893–900 CrossRef Medline
59. Sterkel, A. K., Lorenzini, J. L., Fites, J. S., Subramanian Vignesh, K., Sullivan, T. D., Wuthrich, M., Brandhorst, T., Hernandez-Santos, N., Deepe, G. S., Jr., and Klein, B. S. (2016) Fungal mimicry of a mammalian aminopeptidase disables innate immunity and promotes pathogenicity. *Cell Host Microbe* **19,** 361–374 CrossRef Medline
60. Weber, C., Kraemer, S., Drechsler, M., Lue, H., Koenen, R. R., Kapurniotu, A., Zernecke, A., and Bernhagen, J. (2008) Structural determinants of MIF functions in CXCR2-mediated inflammatory and atherogenic leukocyte recruitment. *Proc. Natl. Acad. Sci. U.S.A.* **105,** 16278–16283 CrossRef Medline
61. Poelarends, G. J., Veetil, V. P., and Whitman, C. P. (2008) The chemical versatility of the β-α-β-fold: catalytic promiscuity and divergent evolution in the tautomerase superfamily. *Cell. Mol. Life Sci.* **65,** 3606–3618 CrossRef Medline
62. Naessens, E., Dubreuil, G., Giordanengo, P., Baron, O. L., Minet-Kebdani, N., Keller, H., and Coustau, C. (2015) A secreted MIF cytokine enables aphid feeding and represses plant immune responses. *Curr. Biol.* **25,** 1898–1903 CrossRef Medline
63. Koga, K., Kenessey, A., Powell, S. R., Sison, C. P., Miller, E. J., and Ojamaa, K. (2011) Macrophage migration inhibitory factor provides cardioprotection during ischemia/reperfusion by reducing oxidative stress. *Antiox. Redox Signal.* **14,** 1191–1202 CrossRef Medline
64. Soares, A. R., Marchiosi, R., Siqueira-Soares Rde, C., Barbosa de Lima, R., Dantas dos Santos, W., and Ferrarese-Filho, O. (2014) The role of L-DOPA in plants. *Plant Signal. Behav.* **9,** e28275 CrossRef Medline
65. Norris, S. R., Shen, X., and DellaPenna, D. (1998) Complementation of the *Arabidopsis pds1* mutation with the gene encoding *p*-hydroxyphenylpyruvate dioxygenase. *Plant Physiol.* **117,** 1317–1323 CrossRef Medline
66. Taddese, B., Upton, G. J., Bailey, G. R., Jordan, S. R., Abdulla, N. Y., Reeves, P. J., and Reynolds, C. A. (2014) Do plants contain G protein-coupled receptors? *Plant Physiol.* **164,** 287–307 CrossRef Medline
67. Pieterse, C. M., Van der Does, D., Zamioudis, C., Leon-Reyes, A., and Van Wees, S. C. (2012) Hormonal modulation of plant immunity. *Annu. Rev. Cell Dev. Biol.* **28,** 489–521 CrossRef Medline
68. Feng, Z., Dubyak, G. R., Jia, X., Lubkowski, J. T., and Weinberg, A. (2013) Human β-defensin-3 structure motifs that are important in CXCR4 antagonism. *FEBS J.* **280,** 3365–3375 CrossRef Medline
69. Saini, V., Marchese, A., and Majetschak, M. (2010) CXC chemokine receptor 4 is a cell surface receptor for extracellular ubiquitin. *J. Biol. Chem.* **285,** 15566–15576 CrossRef Medline
70. Saini, V., Marchese, A., Tang, W. J., and Majetschak, M. (2011) Structural determinants of ubiquitin-CXC chemokine receptor 4 interaction. *J. Biol. Chem.* **286,** 44145–44152 CrossRef Medline
71. Cho, Y., Jones, B. F., Vermeire, J. J., Leng, L., DiFedele, L., Harrison, L. M., Xiong, H., Kwong, Y. K., Chen, Y., Bucala, R., Lolis, E., and Cappello, M. (2007) Structural and functional characterization of a secreted hookworm macrophage migration inhibitory factor (MIF) that interacts with the human MIF receptor CD74. *J. Biol. Chem.* **282,** 23447–23456 CrossRef Medline
72. Pantouris, G., Rajasekaran, D., Garcia, A. B., Ruiz, V. G., Leng, L., Jorgensen, W. L., Bucala, R., and Lolis, E. J. (2014) Crystallographic and receptor binding characterization of *Plasmodium falciparum* macrophage migration inhibitory factor complexed to two potent inhibitors. *J. Med. Chem.* **57,** 8652–8656 CrossRef Medline
73. Borghese, F., and Clanchy, F. I. (2011) CD74: an emerging opportunity as a therapeutic target in cancer and autoimmune disease. *Exp. Opin. Ther. Targets* **15,** 237–251 CrossRef Medline
74. Kraemer, S., Lue, H., Zernecke, A., Kapurniotu, A., Andreetto, E., Frank, R., Lennartz, B., Weber, C., and Bernhagen, J. (2011) MIF-chemokine receptor interactions in atherogenesis are dependent on an N-loop-based 2-site binding mechanism. *FASEB J.* **25,** 894–906 CrossRef Medline
75. Dessein, A. F., Stechly, L., Jonckheere, N., Dumont, P., Monté, D., Leteurtre, E., Truant, S., Pruvot, F. R., Figeac, M., Hebbar, M., Lecellier, C. H., Lesuffleur, T., Dessein, R., Grard, G., Dejonghe, M. J., *et al.* (2010) Autocrine induction of invasive and metastatic phenotypes by the MIF-CXCR4 axis in drug-resistant human colon cancer cells. *Cancer Res.* **70,** 4644–4654 CrossRef Medline
76. Cournia, Z., Leng, L., Gandavadi, S., Du, X., Bucala, R., and Jorgensen, W. L. (2009) Discovery of human macrophage migration inhibitory factor (MIF)-CD74 antagonists via virtual screening. *J. Med. Chem.* **52,** 416–424 CrossRef Medline
77. Boisvert, W. A., Rose, D. M., Johnson, K. A., Fuentes, M. E., Lira, S. A., Curtiss, L. K., and Terkeltaub, R. A. (2006) Up-regulated expression of the CXCR2 ligand KC/GRO-α in atherosclerotic lesions plays a central role in macrophage accumulation and lesion progression. *Am. J. Pathol.* **168,** 1385–1395 CrossRef Medline
78. Soehnlein, O., Steffens, S., Hidalgo, A., and Weber, C. (2017) Neutrophils as protagonists and targets in chronic inflammation. *Nat. Rev. Immunol.* **17,** 248–261 CrossRef Medline
79. Murphy, K., and Weaver, C. (2016) *Janeway's Immunobiology*, 9th revised Ed., pp. 602–627, W. W. Norton and Co., New York
80. Larkin, M. A., Blackshields, G., Brown, N. P., Chenna, R., McGettigan, P. A., McWilliam, H., Valentin, F., Wallace, I. M., Wilm, A., Lopez, R., Thompson, J. D., Gibson, T. J., and Higgins, D. G. (2007) Clustal W and Clustal X version 2.0. *Bioinformatics* **23,** 2947–2948 CrossRef Medline
81. Waterhouse, A. M., Procter, J. B., Martin, D. M., Clamp, M., and Barton, G. J. (2009) Jalview Version 2–a multiple sequence alignment editor and analysis workbench. *Bioinformatics* **25,** 1189–1191 CrossRef Medline
82. Troshin, P. V., Procter, J. B., and Barton, G. J. (2011) Java bioinformatics analysis web services for multiple sequence alignment–JABAWS:MSA. *Bioinformatics* **27,** 2001–2002 CrossRef Medline
83. Whitmore, L., and Wallace, B. A. (2004) DICHROWEB, an online server for protein secondary structure analyses from circular dichroism spectroscopic data. *Nucleic Acids Res.* **32,** W668–W673 CrossRef Medline
84. Whitmore, L., and Wallace, B. A. (2008) Protein secondary structure analyses from circular dichroism spectroscopy: methods and reference databases. *Biopolymers* **89,** 392–400 CrossRef Medline
85. Sreerama, N., and Woody, R. W. (2000) Estimation of protein secondary structure from circular dichroism spectra: comparison of CONTIN, SELCON, and CDSSTR methods with an expanded reference set. *Anal. Biochem.* **287,** 252–260 CrossRef Medline
86. Greenfield, N. J. (2006) Using circular dichroism spectra to estimate protein secondary structure. *Nat. Protoc.* **1,** 2876–2890 CrossRef Medline
87. Rajasekaran, D., Zierow, S., Syed, M., Bucala, R., Bhandari, V., and Lolis, E. J. (2014) Targeting distinct tautomerase sites of D-DT and MIF with a single molecule for inhibition of neutrophil lung recruitment. *FASEB J.* **28,** 4961–4971 CrossRef Medline
88. Dios, A., Mitchell, R. A., Aljabari, B., Lubetsky, J., O'Connor, K., Liao, H., Senter, P. D., Manogue, K. R., Lolis, E., Metz, C., Bucala, R., Callaway, D. J., and Al-Abed, Y. (2002) Inhibition of MIF bioactivity by rational design of pharmacological inhibitors of MIF tautomerase activity. *J. Med. Chem.* **45,** 2410–2416 CrossRef Medline
89. Kelley, L. A., Mezulis, S., Yates, C. M., Wass, M. N., and Sternberg, M. J. (2015) The Phyre2 web portal for protein modeling, prediction and analysis. *Nat. Protoc.* **10,** 845–858 CrossRef Medline
90. Wu, B., Chien, E. Y., Mol, C. D., Fenalti, G., Liu, W., Katritch, V., Abagyan, R., Brooun, A., Wells, P., Bi, F. C., Hamel, D. J., Kuhn, P., Handel, T. M., Cherezov, V., and Stevens, R. C. (2010) Structures of the CXCR4 chemokine GPCR with small-molecule and cyclic peptide antagonists. *Science* **330,** 1066–1071 CrossRef Medline
91. Crump, M. P., Gong, J. H., Loetscher, P., Rajarathnam, K., Amara, A., Arenzana-Seisdedos, F., Virelizier, J. L., Baggiolini, M., Sykes, B. D., and Clark-Lewis, I. (1997) Solution structure and basis for functional activity of stromal cell-derived factor-1; dissociation of CXCR4 activation from binding and inhibition of HIV-1. *EMBO J.* **16,** 6996–7007 CrossRef Medline